Forschungszentrum Jülich
in der Helmholtz-Gemeinschaft

Institut für Schichten und Grenzflächen
Institut 2: Bio- und Chemosensoren

Design and development of radiation-resistant and low-noise semiconductor transistors for applications in high frequency communication systems

Serhiy Danylyuk

Jül-4165

Design and development of radiation-resistant and low-noise semiconductor transistors for applications in high frequency communication systems

Serhiy Danylyuk

Berichte des Forschungszentrums Jülich ; 4165
ISSN 0944-2952
Institut für Schichten und Grenzflächen
Institut 2: Bio- und Chemosensoren Jül-4165
D 82 (Diss., Aachen, RWTH, 2004)

Zu beziehen durch: Forschungszentrum Jülich GmbH · Zentralbibliothek
D-52425 Jülich · Bundesrepublik Deutschland
☎ 02461 61-5220 · Telefax: 02461 61-6103 · e-mail: zb-publikation@fz-juelich.de

Abstract

In the frame of this work, the fundamental properties of GaN/AlGaN HEMT structures have been investigated in order to optimize their performance in high power microwave devices. A number of properties have been studied, starting from DC transport properties in bare 2DEG channels up to investigation of phase noise of a X-band HEMT-based oscillator.

This work is separated into five parts. In the first part, basics of fluctuation phenomena in semiconductors are described along with a discussion of theoretical models, which are most applicable in case of investigation of noise in HEMT devices.

In the second part, a study of 2DEG transport at low and moderate electric fields is performed. The gateless TLM structures have been suggested for adequate analysis of the transport effects. The observed current saturation through a TLM structure confirms that both thermal overheating and hot electron effects are influencing the current. A theoretical model has been developed for the separate investigation of both relevant effects. In order to remove Joule heating effects and to investigate only the fundamental transport properties, a nanosecond pulse measurement technique was developed. By applying 10-30 n*s* electrical pulses to AlGaN/GaN gateless heterostructures, we experimentally measured low field and high field transport phenomena, including the drift velocity dependence on the applied electric field up to the record height of 150 kV/cm for GaN-based heterostructures.

Besides the self-heating, another strong limitation of high frequency devices is low-frequency noise. In the third part, an adequate method for the low-frequency noise sources characterisation from different device regions is proposed and tested for nanoscale Group-III-nitride heterostructures. The temperature dependence of the noise revealed a characteristic transition frequency from the 1/f dependence to a stronger one. The process has activation energy of 0.4 eV, which can be related to traps in the AlGaN barrier.

In the forth part of this work, transport and noise properties of AlGaN/GaN based HEMTs with gate length from 150 nm to 350 nm have been studied before and after gamma irradiation up to $1\text{x}10^9$ Rad doses. The observed changes in the measured HEMTs characteristics were interpreted in terms of additional defects produced by gamma radiation. The noise spectra demonstrate the increasing role of leakage current after high gamma irradiation dose. In general, the results confirm, that due to their high radiation hardness, GaN-based HEMTs have good prospects for stability and reliability of devices intended for application in radiation environment, particularly for space applications.

In the final part of this work, the experience, gained during the investigation of transport and noise properties of the transistors, was used to optimize the parameters of the integrated circuit oscillator. As a result, a low phase noise GaN MMIC oscillator has been presented, in conjunction with the study of the low frequency noise. The oscillator has demonstrated remarkably good performance with low phase noise and high output power. The oscillator delivers an output power of 28 dBm with DC-to-RF efficiency of 16%. The measured phase noise was -105 dBc/Hz at a 100 kHz offset from 9.35 GHz carrier with only 15 MHz/V up conversion factor, which is better then the noise measured for MMIC oscillators built on GaAs HEMTs.

In conclusion, the most important results were summarized, and a perspective for further work towards the development and design of radiation-resistant and low-noise semiconductor components for applications in high frequency communication systems were given.

Kurzzusammenfassung

Im Rahmen dieser Arbeit wurden die fundamentalen Eigenschaften von GaN/AlGaN HEMT Strukturen untersucht, mit Hinblick auf eine Optimisierung Ihrer Leistung für Anwendungen in Hochleistungs-Mikrowellenbauteilen. Die studierten Eigenschaften reichten von der Untersuchung grundlegender Gleichstrom-Transporteigenschaften in 2D-Elektronengas-Kanälen bis hin zur Untersuchung des Phasenrauschens eines X-Band HEMT-basierten Oszillators.

Die Arbeit ist in fünf Teile unterteilt: Im ersten Teil werden die Grundlagen von Fluktuationsphänomenen in Halbleitern beschrieben zusammen mit einer Diskussion mehrerer theoretischer Modelle, die zur Beschreibung von Rauschen in HEMT-basierten Bauteilen geeignet sind.

Im zweiten Teil wird eine Studie von 2DEG Transporteigenschaften bei niedrigen und moderaten elektrischen Feldern durchgeführt. Für eine adäquate Analyse der Transporteffekte werden gate-lose TLM Strukturen herangezogen. Die beobachtete Stromsättigung durch eine TLM-Struktur bestätigt, dass sowohl thermische Überhitzung als auch Effekte heißer Elektronen den Strom beeinflussen. Um Joule'sche Aufheizungseffekte zu verhindern und nur die fundamentalen Transporteigenschaften zu messen wurde eine Nanosekunden-Pulsmesstechnik entwickelt. Durch Anlegen elektrischer Pulse mit 10-30 ns Pulslänge an AlGaN/GaN Heterostrukturen wurden experimentell Transportphänomene bei niedrigem und hohem Feld gemessen, einschließlich der Abhängigkeit der Driftgeschwindigkeit vom angelegten Feld bis hin zu einer Rekord-Feldstärke von 150 kV/cm für GaN-basierte Heterostrukturen.

Ein starker Nachteil von Hochfrequenz-Bauteilen ist neben Selbstaufheizungseffekten das Niedrigfrequenzrauschen. Im dritten Teil der Arbeit, wird eine geeignete Methode zur Charakterisierung von Niedrigfrequenzrauschquellen vorgeschlagen und für nanometergrosse III-Nitrid Heterostrukturen getestet. Das Temperaturverhalten der Rauscheigenschaften enthüllt eine charakteristische Übergangsfrequenz von 1/f Rauschen zu einer stärkeren Rauschquelle. Dieser Prozess mit einer Aktivierungsenergie von 0.4 eV kann auf Elektronenfallen in der AlGaN Barriere zurückgeführt werden.

Im vierten Teil dieser Arbeit werden Transport- und Rauscheigenschaften von AlGaN/GaN basierten HEMTs mit Gatelängen von 150 nm bis 350 nm vor und nach Bestrahlung mit Gammastrahlung einer Dosierung bis zu $1x10^9$ Rad bestimmt. Die beobachteten Veränderungen in den Charakteristika der gemessenen HEMTs wurden mittels der Entstehung zusätzlicher Defekte durch die Gamma-Bestrahlung interpretiert. Im allgemeinen bestätigen die Resultate, dass aufgrund ihrer hohen Strahlungsbeständigkeit GaN-basierte HEMTs gute Aussichten in Bezug auf Stabilität und Zuverlässigkeit für Bauteile, die in strahlungsbelasteter Umgebung und speziell für Raumfluganwendungen gedacht sind.

Im letzten Teil der Arbeit wurde die Erfahrung, die während der Untersuchung der Transport- und Rauscheigenschaften der Transistoren gemacht wurde genutzt, um die Parameter eines integrierten Oszillatorschaltkreises zu optimieren. Dabei wurde ein GaN MMIC Oszillator mit niedrigem Phasenrauschen präsentiert, in Verbindung mit der Studie des Niederfrequenzrauschens. Der Oszillator liefert eine Ausgangsleistung von 28 dBm mit einer DC-zu-RF Konversionseffizienz von 16%. Das gemessene Phasenrauschen betrug -105 dBc/Hz bei einer Offsetfrequenz von 100 kHz neben einem Träger bei 9.35 GHz, was die Rauschwerte von MMIC Oszillatoren auf GaAs-HEMT Basis übertrifft.

Schliesslich werden die wichtigsten Ergebnisse zusammengefasst und ein Ausblick für zukünftige Arbeit mit Hinblick auf die Entwicklung und das Design strahlungsbeständiger rauscharmer Halbleiterkomponenten für Anwendungen in Hochfrequenz-Kommunikationssystemen wird gegeben.

Introduction

Modern semiconductor electronics and optoelectronics demand the development of novel material systems and optimization of their properties for a wide range of applications. For most of these applications silicon has established itself as the material of choice, due to its availability, price and universal physical properties, such as easy material processing, decent carrier mobility, good thermal conductivity etc. With further development of industry and science, however, a number of challenges emerged, where other material systems are vastly outperforming silicon, or silicon cannot be used at all. These include the development of optical devices like light emitting devices (LED) or lasers, high performance and high power electronics as well as low noise and radiation resistant devices. During the last decades a number of different material systems were suggested and successfully implemented, among which one the most recent ones are group III- nitrides compounds.

With the development of wireless telecommunication, high-speed cellular networks and aerospace systems, the demand for solid-state power amplifiers and high power oscillators has been continually increasing. These devices require increasing performance in terms of high power level, efficiency, linearity and operating frequency as well as low-noise demands and good thermal and radiation stability. The existing materials and technologies often cannot match these demands. For example, GaAs-based power devices have been very reliable at high frequencies up to tenth of GHz. However, their power performances have already been pushed close to the theoretical limit. In terms of power density, about 1 W/mm at 10 GHz would be the state of the art performance for GaAs pseudomorphic high electron mobility transistors (pHEMTs). Under such circumstances, wide band-gap semiconductors with a higher breakdown voltage along with good electrical, thermal and noise properties are needed. For many years, silicon carbide (SiC) has been widely seen as a potential candidate, but unfortunately it doesn't fulfil the requirements in terms of electrical properties. With technological and cost advantages, the Gallium Nitride (GaN) based family of semiconductor has quickly gained a lot of attention. In terms of electronic material properties, GaN possesses very attractive features such as a large band-gap (3.4 eV), high breakdown fields ($3x10^6$ V/cm) and extremely high peak ($3x10^7$ cm/s) and saturation electron velocity ($2x10^7$ cm/s). Unique polarization induced interface charges in AlGaN/GaN heterostructures cause high carrier concentrations ($\sim10^{13}cm^{-2}$) of the two-dimensional electron gas (2DEG) without additional doping. This leads to reduced scattering and consequently, to increased room temperature mobility (up to 1500 cm^2/Vs)[1]. GaN epitaxial layers can be grown on single-crystal sapphire (Al_2O_3) and SiC substrates. Sapphire has the advantage of lower cost and the availability of larger wafer size than SiC, but it is not as good as a thermal conductor. GaN HEMTs on SiC have achieved a power density of 7-12 W/mm [2],[3], while GaN HEMTs on sapphire have demonstrated 4.8-6.6 W/mm [3],[4], and the difference is believed to be due to the higher thermal conductivity of SiC (σ = 450 W/mK) over sapphire (σ = 30 W/mK).

However, the two-dimensional electron gas (2DEG) transport in HEMTs is strongly affected by a variety of other factors: proximity to the surface, surface conditions, the channel non-uniformity, etc. To use group III-nitride heterostructures in high power and high temperature microelectronic applications, all of these should be investigated in detail. Additionally, high-field transport properties of nitride materials of relaxation mechanisms of hot carriers, intervalley transfer and the velocity-field characteristics have not been studied so far in detail. There are no experimental measurements of the velocity-field characteristics in two-dimensional III-V nitride based heterostructures at electric fields close to the critical one in this material system. This information on hot carriers is of fundamental importance for the performance of all semiconductor electronic devices. On the other hand, continual increase of number and speed of wireless data transmission systems sets up the demand for very low noise microwave components. While the main source of phase noise in HEMT-based amplifiers is due to the upconversion of low-frequency *1/f* amplitude noise, the study of the fundamental properties of *1/f* noise in HEMT structures gains high importance. With limited systematic investigations available it offers a large new field of both practical and fundamental research.

Noise level in multi component systems is strongly dependent on the noise level of each element, the impedance-parameter matching between the elements and the degree of nonlinearity. The main nonlinear element of an oscillator is the active device, its noise behaviour depends on several factors: layer structure and processing design, operating voltages, heating effects, variation of parameters with temperature and other external factors: magnetic fields, radiation surrounding, optical excitation, etc. Therefore it is extremely important for the design of an ultra low noise oscillator to look for ways of the nonlinear device optimisation.

In the frame of this work, the fundamental properties of GaN/AlGaN HEMT structures have been investigated in order to optimize their performance in high power microwave devices. A number of properties have been studied, starting from direct current (DC) transport properties in bare 2DEG channels up to the investigation of phase noise of a X-band HEMT-based oscillator.

This work is separated into five parts. In the first part, basics of fluctuation phenomena in semiconductors are described along with a discussion of theoretical models, which are most applicable in the case of investigations of noise in HEMT devices.

In the second part, a study of 2DEG transport at low and moderate electric fields is performed. A new tool for the investigation of transport in heterostructures is suggested: gateless transmission line model (TLM) structures. Transport peculiarities in group-III nitride-based (AlGaN/GaN) heterostructures grown on sapphire for HEMT applications studied in details as in low and moderate fields as well as in high (up to 150 kV/cm) electric fields in the pulse regime. Effects of self-heating and its influence on transport properties in the structures are carefully investigated both theoretically and experimentally. A new method of investigation of self-heating and hot-electron effects in the same experiment is developed.

In the third part, an adequate method for the low-frequency noise source characterisation from different device regions is proposed and tested for nanoscale Group-III-nitride heterostructures. The revealed behaviour of the noise spectra as well as the small value of the Hooge parameter is discussed within theoretical models of the noise associated with specific resistance fluctuations. Additionally, a study of the noise spectra of leakage current has been performed. Generation-recombination (GR) features in the spectra was revealed and attributed to the current flow through the AlGaN barrier region. Parameters of the GR process were estimated from the analysis of the noise spectrum. The temporal dependence of leakage current behaves like random telegraph signal (RTS), which provides additional information about the GR process. Two different RTS series in the current were observed. The importance of reducing the interaction between channel electrons and barrier states is confirmed.

In the fourth part of this work, transport and noise properties of AlGaN/GaN based HEMTs with gate lengths from 150 nm to 350 nm have been studied before and after gamma irradiation. The observed changes in the measured HEMT characteristics are interpreted in terms of additional defects produced by gamma radiation. The noise spectra demonstrate the increasing role of leakage current after gamma irradiation. The Hooge parameters determined separately for passive ($\sim 1x10^{-3}$) and active (about $5x10^{-4}$) regions of the device show values three to five times larger after a radiation dose of $2x10^{8}$ Rad. However, it was shown that transport and noise characteristics of the transistors reveal a tendency to improvement under irradiation by gamma-quanta up to doses of 10^{6} Rad. The effect is explained by relaxation of elastic strains and structural ordering of native defects in the AlGaN barrier layer. The suggestion is confirmed by results of structural characterization of as-grown heterostructures after the same radiation treatment. In general, results confirm, that due to their high radiation hardness, GaN-based HEMTs show good prospects for stability and reliability of devices intended for application in harsh radiation environment, such as space applications.

In Chapter 5 results from studies made in Chapter 2-4 were used to optimize the parameters of an X-band oscillator based on an AlGaN/GaN HEMT. A high power voltage-controlled oscillator has been built and characterized in details. Oscillator has shown excellent phase noise performance together with high output power. The oscillator delivers an output power of 28 dBm with a DC-to-RF efficiency of 16%. The measured phase noise is –105 dBc/Hz at 100 kHz offset from 9.35 GHz carrier. This level of noise is a record up to date for MMIC X-band oscillators regardless of the basis material.

Finally, the most important results are summarized, and a perspective for further work towards the development and design of radiation-resistant and low-noise semiconductor components for applications in high frequency communication systems are given.

Chapter 1: Fluctuation phenomena in semiconductor materials and devices

For a long time fluctuation phenomena in semiconductor materials and devices were considered only as a limitation to sensitivity and performance of devices. Therefore, all investigations in this field were application-driven and directed towards understanding the origin of fluctuation to be able to reduce the noise level and increase sensitivity and stability of devices. A number of problems arose during the studies that appeared to be quite complex and difficult to solve.

Thanks to these investigations, two important facts were discovered. It was found that reducing of a noise level does not necessarily increase a sensitivity or performance. This fact leads to conclusion that the origins of noise often strongly bound to the basic physical mechanisms in the device, which are responsible for its operation. As a matter of fact, these are the same factors that determine the level of the "useful" signal. Hence the results of noise investigations can give valuable information about the different physical processes occurring in semiconductor materials and devices. In other words, studying of noise phenomena can be used not only to determine noise parameters of structure or device but also to investigate their non-noise properties and characteristics.

The second important outcome of the first noise investigations is high sensitivity of noise generation process to particular physical feature of the given device, even if this feature does not visible in non-noise characteristics of a device. This means that the noise study may serve as a very sensitive method of investigation and makes it possible to obtain additional information about semiconductor materials and structures that is not accessible by other physical methods.

Thus, the study of noise may be used not only to improve the device sensitivity but also to examine different physical phenomena and to determine various semiconductor parameters.

1.1 General noise theory

Fluctuation phenomena, also called as noise, occur in semiconductors due to the statistical nature of different physical processes in these materials.

In general, when a quantity X shows noise we may write:

$$X(t) = \langle X \rangle + \Delta X(t) \tag{1.1}$$

The symbol $\langle X \rangle$ means averaging over a long period of time. Now $\Delta X(t)$ may be written in a Fourier series:

$$\Delta X(t) = \sum a_i \exp(j2\pi f_i t) + a_i^* \exp(-j2\pi f_i t) \tag{1.2}$$

where the coefficients a_i are fluctuating amplitudes. The noise component measured at a frequency f_i is then

$$\langle \Delta X_i \rangle = 0 \tag{1.3}$$

$$\langle (\Delta X_i)^2 \rangle = 2\langle a_i a_i^* \rangle \tag{1.4}$$

If we are measuring in a finite bandwidth Δf, the Fourier components inside the bandwidth add up quadratically. Such a noise, measured in a unit of bandwidth is called the spectral density . For a steady state process the value of spectral density is determined as follows [5],[6],[7]:

$$S_X(f) = \lim_{T\to\infty} 2T\left\langle a_i a_i^* \right\rangle \quad (1.5)$$

Here asterisk denotes the complex conjugate of the quantity involved.

Another basis parameter in noise theory is so called autocorrelation function $\varphi_X(t)$. $\varphi_X(t)$ describes how, on the average, a deviation $\Delta X(t_0)$will decay. The autocorrelation function is defined by

$$\varphi_X(t) = \left\langle \Delta X(t_0)\Delta X(t_0+t)\right\rangle \quad (1.6)$$

$\varphi_X(t)$ and $S_X(f)$ connected by the Wiener-Khintchine relations[8],[9]:

$$S_X(f) = 4\int_0^\infty \varphi_X(t)\cos 2\pi ft\,dt \quad (1.7)$$

$$\varphi_X(t) = \int_0^\infty S_X(f)\cos 2\pi ft\,df \quad (1.8)$$

These equations are used when making a physical model for an observed noise.

There are three well understood types of noise that are frequently seen in noise spectra: thermal noise, shot noise and generation-recombination noise.

(a) Thermal noise.

The statistical nature of the scattering of free charge carriers causes random changes in their velocities and, hence, random microscopic diffusion currents. In equilibrium situation this motion has an average energy of $\frac{1}{2}kT$. As a result, a fluctuating current that is equal to the sum of these microcurrents exists in semiconductor samples and a fluctuating voltage is observed at their electrical contacts (Brownian motion noise). Under thermal equilibrium conditions, this noise is called thermal noise or Johnson noise [10],[11]. In a more general case it is called diffusion noise.

In terms of resistance it means that any resistance R shows spontaneous current fluctuations or voltage fluctuations governed by the equations:

$$S_V = 4kTR \tag{1.9}$$

or

$$S_I = 4kT/R \tag{1.10}$$

This white spectrum is always found, whatever the nature of the conduction process, or the nature of the mobile charge carriers. Thermal noise is generated in any dissipative physical resistor.

(b) Shot noise.

Charge transfer in semiconductor often connected with overcoming of different potential barriers. For example, electrons emitted from a hot cathode in a vacuum diode, or electrons, crossing potential barrier in heterostructure – these carriers are randomly generated. Random generation leads to fluctuation around the average current *I*:

$$S_I = 2eI \tag{1.11}$$

Schottky [12] was the first to consider such a noise. It worth to note that shot noise is a non-equilibrium phenomenon associated with current flow in a driven stationary state. The spectrum is white at all attainable frequencies because of the very high transit time of the electrons.

(c) Generation-Recombination (GR) noise.

The number of free electrons in the conduction band may fluctuate because of generation and recombination processes between the band and traps. The appearance and disappearance of carriers in a semiconducting sample by the processes of generation and recombination is described by a differential equation [13]:

$$-\frac{d\Delta N}{dt} = \frac{\Delta N}{\tau}, \tag{1.12}$$

where ΔN is the fluctuation in the number of carriers and τ is the lifetime of added carriers. Then the autocorrelation function, according to Eq. (1.6) will be:

$$\varphi_N(t) = \langle \Delta N(t_0) \Delta N(t_0 + t) \rangle = \left\langle \{\Delta N(t_0)\}^2 \right\rangle \exp(-t/\tau) = \left\langle (\Delta N)^2 \right\rangle \exp(-t/\tau) \qquad (1.13)$$

The Wiener-Khintchine theorem (Equations (1.7)-(1.8)) then gives:

$$S_N(f) = \left\langle (\Delta N)^2 \right\rangle \frac{4\tau}{1 + (2\pi f \tau)^2} \qquad (1.14)$$

This type of spectrum is called Lorentzian. If there is only one type of trap, then the variance $\left\langle (\Delta N)^2 \right\rangle$ is given by:

$$\frac{1}{\left\langle (\Delta N)^2 \right\rangle} = \frac{1}{N} + \frac{1}{X_n} + \frac{1}{X_p} \qquad (1.15)$$

where X_n is the average number of occupied traps and X_p the average number of empty traps. The variance thus approximates the smallest of the quantities N, X_n and X_p.

1.2. 1/f Noise.

There is, however, another type of noise that is often seen on spectra but did not have simple unified theory behind. It is *1/f* noise – fluctuation in the conductance with a spectral density proportional to $f^{-\gamma}$, where $\gamma = 1.0 \pm 0.1$ in a wide frequency range, usually measured in the range from 1Hz to 100 kHz. It is clear that the spectrum $\frac{S_I}{I^2} \sim \frac{1}{f}$ cannot be exactly $1/f$ in the whole range $0 < f < \infty$. Firstly, $S \to \infty$, when $f \to 0$. Also, the integral of $S \to \infty$ at both frequency limits $f = 0$ and $f = \infty$. There fore, if noise is stationary the spectrum must flatten below a certain low frequency and it must become steeper above a certain high frequency. Neither of these frequency limits has ever been observed. High frequency limit is masked by thermal noise usually and practically not reachable. For low frequency limit observation two solutions are possible: (a) the noise is not stationary, or (b) we must measure at still lower frequencies. Second choice is hard to perform, as measurements at frequencies around 10^{-6} Hz will need around a month to be completed.

Unlike the first three sources mentioned above, which are well understood, a the origin of the *1/f* noise is still open to debate [14],[15],[16]. At the moment, two theoretical approaches to describing the *1/f* noise are discussed: the McWorter and Hooge models. The main physical difference between these two cases is the origin of noise sources. McWorter's model of the noise deals with surface or interface noise sources (fluctuations of concentration, Δn) [17], while Hooge's model takes into consideration the distribution of noise sources in the volume (mobility fluctuations, Δμ) [18]. The question whether Δn or Δμ is responsible for current fluctuations in HEMTs even in the case of equilibrium (low voltage) noise still remains open. In the next two sessions both theories will be described in detail.

1.2.1 The McWhorter model.

First relatively successful attempt to give a simple physical model for *1/f* noise has been done by McWhorter back in fifties [19],[20]. After almost 50 years this theory has remained the most accepted model in metal-oxide-semiconductor transistors (MOST) and HEMTs.

In this theory trapping of charge carriers in traps located at a distance from the semiconductor-oxide (for MOST) or hetero- (for HEMTs) interface is considered as the noise source. Fluctuation of resistance, in this theory, is caused by fluctuation of number of free charge carriers due to trapping/detrapping processes.
Formation of *1/f* spectra in this theory can be explained as follows. As follows from the Eq. (1.14), in case of capturing of charge by a trap with a single capture time τ, the resulting noise spectrum will have a Lorenzian shape (GR noise). Schematically the spectra for two traps with slightly different capture time are shown at Fig. 1.1.

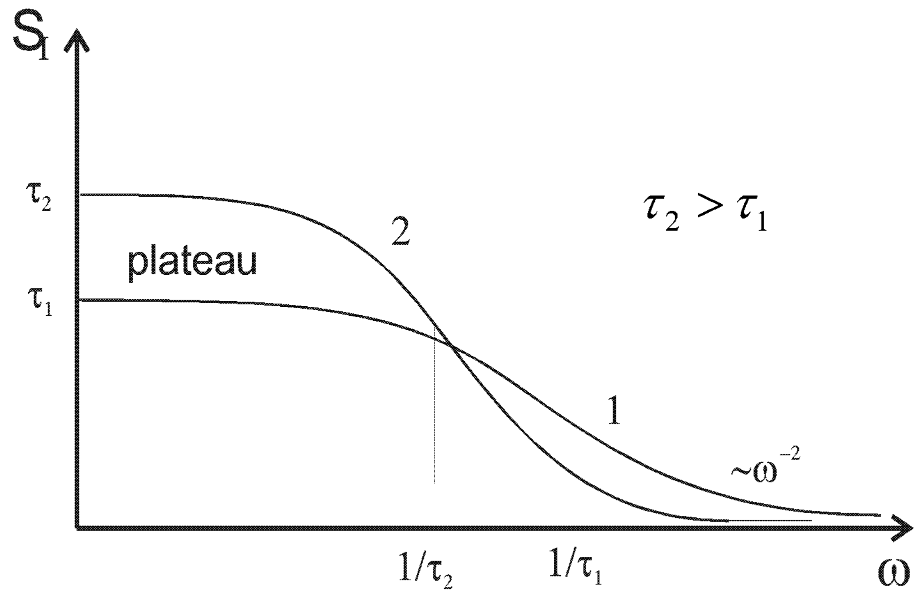

Figure 1.1. Single capture time constant τ : GR noise, Lorentzian spectrum.

The noise spectra in terms of cyclic frequency $\omega = 2\pi f$ will be described by expression:

$$\frac{S_I^0(\omega)}{I^2} = \frac{4N_{te}}{AN^2}\frac{\tau}{1+\omega^2\tau^2}, \tag{1.16}$$

where A - area of the interface, N_{te} -number of traps that can capture electrons and N – total number of electrons.

However, if you assume that in vicinity of your interface traps are uniformly distributed (for example, they have the same energy but uniformly distributed in distance from the interface, or *vice versa*) then one can write a following expression for capture time of these traps:

$$\tau = \tau_0 \exp(\beta y), (y < 0) \tag{1.17}$$

where y – distance from interface to the trap.

In this case unified noise spectra from these traps will form *1/f* dependence in a broad frequency range (Fig. 1.2). Corresponding transformation of equation (1.16) yields a following formula for noise spectra in case of uniformly distributed traps:

$$\frac{S_I^0(\omega)}{I^2} = \frac{N_{te}}{N^2 A \ln(\tau_2/\tau_1)} \frac{1}{f} \tag{1.18}$$

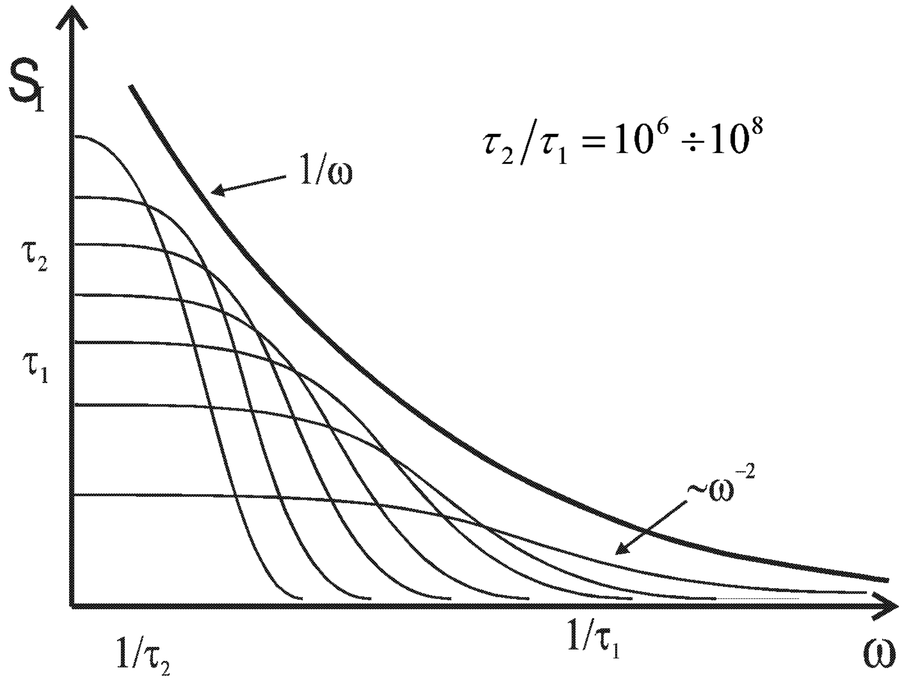

Figure 1.2. Distributed time constant: $1/f$ *noise*

This simple and beautiful theory attracted a lot of scientific attention. However, *1/f* noise appeared also in materials, where existence of surface or interface traps was very unlikely, for example, in continuous metals films [21]. Therefore with time it failed to be a general theory of *1/f* noise, while still holding a place of most popular theory in case of MOSTs and HEMTs.

1.2.2 The Hooge model.

In 1969 Hooge proposed [22] an empirical relation for the *1/f* noise in homogeneous samples:

$$\frac{S_R}{R^2} = \frac{\alpha}{Nf} \tag{1.19}$$

It was done in an effort to explain systematically collected data on *1/f* noise from literature. The only theoretical idea behind the relation (1.19) was that whatever the electrons do when producing *1/f* noise, they do independently. Thus α is a normalized measure for the relative noise in different materials, at different temperatures, etc. There was no reason to assume that α is constant. However, experimental results show that the values of α were not too far apart, mostly in the range of $\alpha = 2 \times 10^{-3}$. Later it was found, that α depends on the quality of crystal and on the scattering mechanisms that determine mobility μ.

In contrast to equation (1.18), (1.19) does not hold any dimensions length, width or thickness, therefore the noise, governed by (1.19) considered to be bulk noise. The same formula was found to work for point contacts [23] and metal films [24], breaking the image of *1/f* noise as purely semiconductor effect.

At the present time, the relation (1.19) is widely acceptable in many types of structures. α has been established as measure of “noisiness” of a structure and usually referred as α_H - Hooge constant.

The primary difference of Hooge model is that Hooge noise is bulk effect and experimentally found to be inversely proportional to the total number of free carriers. This excludes surface effects as a source of Hooge noise. Another difference is the approach to conductivity fluctuations. In contrast to McWhorter theory, Hooge model says that conductivity fluctuations are caused not by concentration variance but by mobility fluctuations.

Experimental investigations show that the lattice scattering of free carriers most likely is the origin for such fluctuations.

Several attempts to build an appropriate theory for empiric Hooge findings have been performed. Most successful today are the theories of local interference noise by P. Dutta and P.M. Horn [25] and quantum *1/f* noise by P.H. Handel [26]. First theory proved to be reliable in case of noise in metals while second is very general theory of *1/f* noise applicable to all type of devices.

Detailed description of these theories is beyond the scope of this chapter. All of them are dealing with interference of electron waves. In local interference theory the interference comes from the waves scattered at many centres (lattice defects, etc). When the spatial arrangement of the centres changes, we observe a change in the conductance, noise. Handel theory is more general – there are *1/f* fluctuations in each individual scattering event at each individual scattering centre. Interference occurs between the Bremstrahlung and non-Bremstrahlung part of the electron wave function.

It should be noted that α values predicted by Handel [27],[28] are of the order of 10^{-8}-10^{-9}. This corresponds to experimental values only for few particular cases. In semiconductors the values of α mostly at 10^{-3} – 10^{-5} range [29]. This could mean that usually in semiconductor devices and structures there are other mechanisms of noise in addition to the predicted by Handel's theory. This topic, however, is still open to discussion.

Chapter 2: Low- and high-field transport properties of AlGaN/GaN heterostructures

In order to optimize a parameters of transistor for use in high power high frequency devices we shall start with investigation of their basic transport properties. A number of non-trivial effects can influence performance of HEMTs both at low and high operating powers. For high power operation the self-heating effects should also be taken into account. The dominating mechanisms of energy and impulse relaxation also need to be investigated.

This chapter addresses the study of two-dimensional electron gas (2DEG) transport at low and moderate electric fields. The devices under study are Group-III nitride-based (AlGaN/GaN) heterostructures grown on sapphire for HEMT applications. For investigation the transport properties of these devices we suggested a use of the transmission line model (TLM) patterns of different channel lengths, L and the same channel width. These structures normally used for determination of contact resistance. The main difference from processed HEMT structure is the absence of gate electrode. In this case the voltage drop in the structure practically linear that allows us simple recalculation of applied to the structure voltage V to electric field in the structure E.

DC and pulsed measurements of these structures revealed a number of features, important for further optimization. Unique drift velocity data has been obtained at ultra-high field measurements.

2.1 Self-heating and hot-electron effects in AlGaN/GaN heterostuctures.

It has been established that at the AlGaN/GaN heterointerface a conducting channel is formed with two-dimensional electron gas (2DEG). A high electron concentration in the channel is achieved without intentional doping due to large polarization fields inherent in the nitride material system [30]. Both experimental and theoretical investigations [31,32] indicate that the electron transport in the conducting channels reveals a number of properties quite different from what has been observed in other III-V heterostructures.

High sheet carrier concentrations (in excess of 10^{13} cm^{-2}) and large values of the carrier mobility and breakdown voltages (power densities are in the few W/mm range) make necessary for better understanding transport properties to take into consideration self-heating phenomenon, when the channel is heated by dissipated power [33,34]. Since the carrier mobility is dependent on both electric field strength and lattice temperature, two effects are present simultaneously: the effect of hot electrons and Joule self-heating of the lattice. A distinguish can be made by studying the change in transport characteristics by varying dissipated power at the same values of the electric field strength.

2.1.1. Experimental details

The investigated devices are fabricated from GaN/AlGaN (33% Al) undoped heterostructures of 1.1 μm GaN and 23 nm AlGaN covered with 320 nm Si_3N_4 passivation layer. The TLM structures are patterned on the same wafer as used for HEMT device formation grown by metal organic chemical vapor deposition on sapphire with 40 nm AlGaN (16% Al) intermediate nucleation layer. The conducting channel of devices is of 100 μm width with the length L scaled to varied distance as 1, 5, 15, 20, and 25 μm. The TLM ohmic contacts were processed by Ti/Al/Ti/Au metallization annealed for 40 s at 800 °C. Schematically structure design is shown on Fig.2.1.

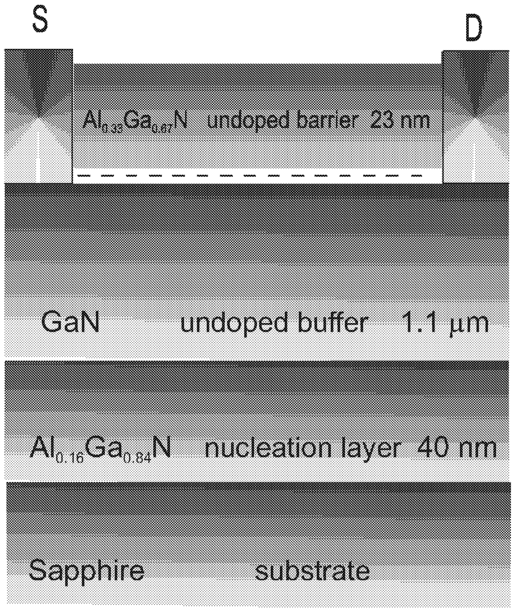

Figure 2.1. Schematic layout of the sample under investigation.

A room temperature mobility of 1250 cm^2/Vs at a sheet carrier density of $1.05x10^{13}$ cm^{-2} has been measured in the 2DEG of the channel by means of Van der Pauw method. Current-voltage (*I-V*) characteristics have been measured in steady-state and transient current conditions with time step as low as 10^{-6} s.

2.1.2 DC and pulsed I-V measurements

Obtained current-voltage characteristics of the samples with different sample length are shown in Fig.2.2. Taking into account voltage drop on contact and normalizing these dependencies on channel length, on can build a current-field dependence (*I*-E) (Fig.2.3.)

Here $E=V/L$ being an average electric field in the conducting channel, V the applied voltage and L – length of the channel. Both pulsed and DC measurements show dependence of the current on the channel length. The longer the channel, the greater the observed difference between DC and pulsed *I–E* characteristics. With increasing L a portion on the *I–E* curve with saturation current manifests itself in the range of measured electric field (voltage) less than 8 kV/cm. It should be noted that the regime of operation with saturation current for AlGaN/GaN TLM structures is reported for the first time. Importantly, the latter regime is not associated with a gate region as it usually takes place in HEMT devices for similar range of the applied voltages.

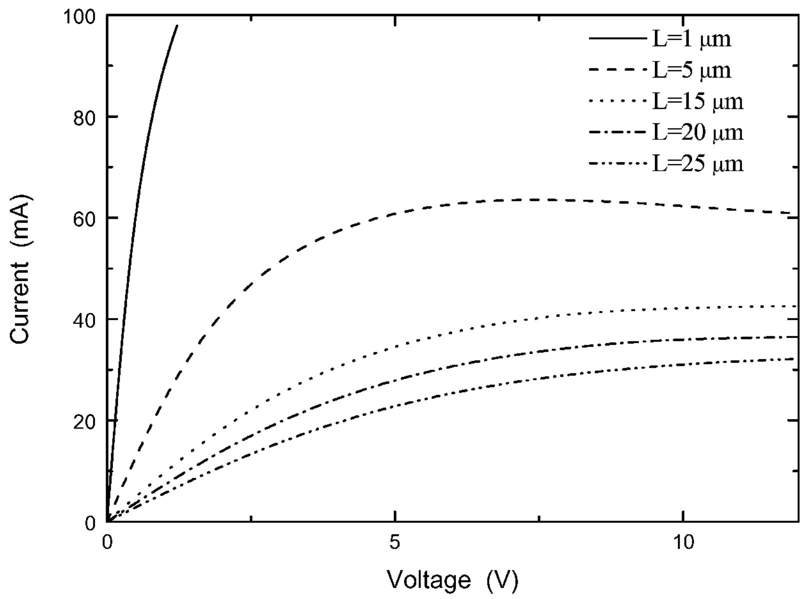

Figure 2.2. Measured I-V characteristics of the channel current with different length of channel

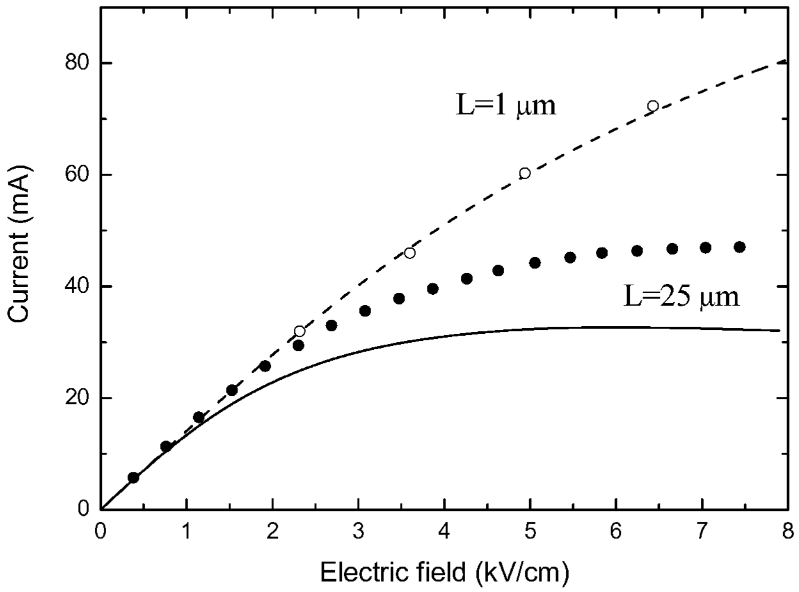

Figure 2.3. Measured DC (lines) and 1 μs pulse (circles) measurements of the current-electric field dependence in shortest and longest channels

2.1.3 Thermal management model

In general, the obtained *I–E* characteristics are strongly nonlinear although the considered field range (< 8 kV/cm) is well below the fields of hot-electron non-ohmic behavior expected from theoretical predictions [35].

For description of the observed behavior of the *I–E* characteristics we develop a simple theoretical model based on (i) heat dissipation and thermal path modeling in the device and (ii) self-consistent solution of coupled nonlinear equations for the channel current I and the channel temperature T. It is determined by dissipated power P_{dis} and heat conduction properties in the device. We suppose that thermal impedance is primarily determined by the sapphire substrate (see Fig. 2.4) [33]. If we neglect for simplicity the temperature dependence in the thermal conductivity of the substrate, $\lambda(T)$, the problem is reduced to the Laplace equation.

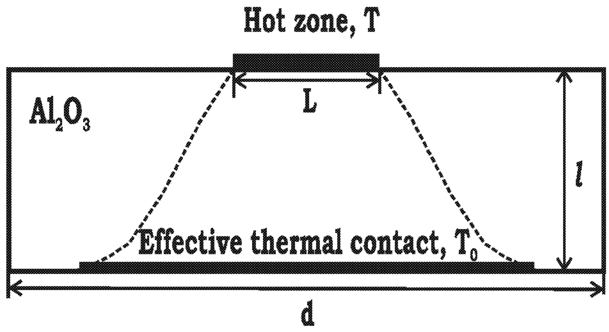

Figure 2.4. Considered model of a heat dissipation in the structure

The boundary conditions can be set as a constant heat flux $q = P_{dis}/(WL)$ from hot zone (conducting channel) on the top of the substrate; adiabatic thermal conditions all over the remainder surface (q =0), except the bottom where an isothermal condition is provided by good thermal contact under certain temperature T_0. These allow us to find temperature distribution in the substrate and evaluate the channel temperature, T, averaged over the channel area, $S_{ch} = WL$ (see Appendix). The temperature rise $\Delta T = T - T_0$ in the channel is related to P_{dis} through the thermal impedance $\theta = \Delta T/P_{dis}$. The latter can be written as

$$\theta = l/\lambda S_{eff}, \qquad S_{eff} = d^2/[1+\sigma(L/d, W/d, l/d)], \qquad (2.1)$$

with the function $\sigma = 2(\sigma_1 + 2\sigma_2)$ being expressed in terms of infinite series [36]:

$$\sigma_1 = \sum_{n=1}^{\infty}\{\varphi_n^2(W/d) + \varphi_n^2(L/d)\psi_{n=m}(l/d\sqrt{2})\}$$

$$\sigma_2 = \sum_{n,m=1}^{\infty}\varphi_n^2(L/d)\varphi_m^2(W/d)\psi_{nm}(l/d)$$

For $L = W = d$ we get $\sigma = 0$ and $S_{eff} = S = d^2$. Then (2.1) reduces to the thermal impedance under a one-dimensional heat conduction. For $(W, L) < d$, we get $\sigma > 0$ and respectively S_{eff} <

S, which leads to an increase in the thermal impedance due to three-dimensional character of the heat conduction.

The current I as a function of electric field E can be determined from coupled equations:

$$I = e\mu(T_0 + \Delta T, E)NWE\,, \tag{2.2}$$

$$\Delta T = \theta(T_0, L)IEL\,. \tag{2.3}$$

Here e is the electron charge, μ the electron mobility, N the sheet electron concentration in the conducting channel. Below numerical solutions to Eqs. (2.2)-(2.3) are found taking advantage of the above thermal impedance, as well as the recent results on Monte Carlo simulation of 2D electron transport [35] and experimental study of the low field mobility on temperature at elevated temperatures in nitride heterostructures [7]. Specifically, we take for the field dependence of the electron mobility $\mu(T, E) = \mu_0\,(T)/[1 + \varsigma\,(E/E_c)^{\,\beta}]$, with β, ς, and E_c being fitting parameters [35]. The low field electron mobility is taken to be [37] $\mu_0(T) = \mu_{300}\,(300/T)^{1.8}$, where μ_{300} is the electron mobility at room temperature.

The equations from (2.1) to (2.3) allow us to calculate the current I and temperature rise ΔT as a function of the electric field E in the channels with different lengths L. The results of calculations I vs E for L = 1 µm and 25 µm are presented in Fig. 1.5 by dashed and dotted curves.

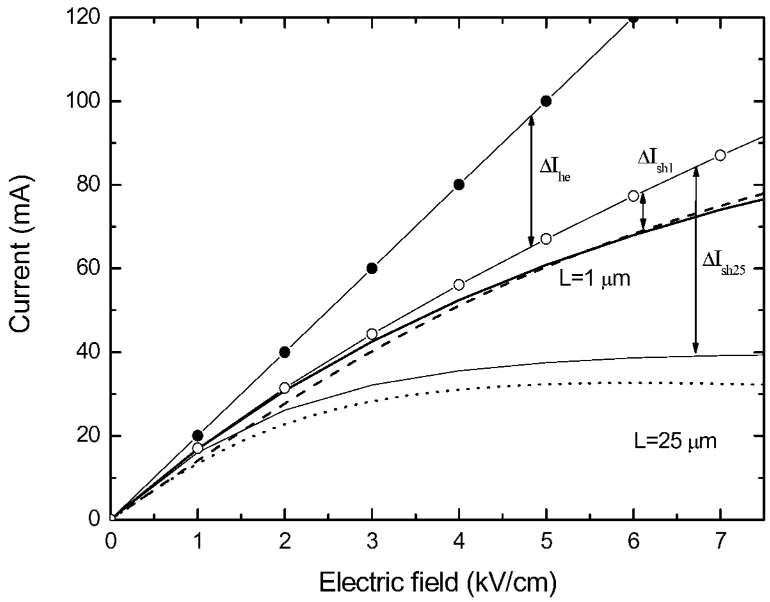

Figure 2.5. Comparison of experimental (dashed and dotted lines) and calculation results (solid lines) independent on T)

The thermal impedances θ_1 = 43 Kmm/W and θ_{25} = 24 Kmm/W have been obtained from (1) for L = 1 μm and 25 μm, respectively, using the substrate parameters d = 1.5 mm, l = 300 μm, λ = 0.33 W/cmK. These values agree well with the thermal impedance of 25 Kmm/W obtained for AlGaN/GaN HEMTs grown on sapphire [33]. As is seen from Figure 2.5, the computational results are in a good agreement with the experimental data. In particular, at the electric field value of 8 kV/cm we obtain the temperature rise ΔT = 27 K at P_{dis} = 0.64 W/mm for the channel with L = 1 μm, and ΔT = 144 K at P_{dis} = 6 W/mm for L = 25 μm. Respectively, the self-heating effect results in 14% and 51% of current reduction for 1 μm and 25 μm length conducting channels. Note that for long channels this leads to negative differential slope for both experimental and calculated I–E curves. Since characteristic times determining the self-heating kinetics in epilayer structure and substrate may differ in several orders of magnitude [33], the pulsed measurements in 10^{-6} s regime exhibit a partial self-heating. The comparison between the calculated and experimental I–E dependences for the device with L = 25 μm (Fig. 2.5) indicates that only 60% of the full (DC) temperature rise is reached in these measurements.

The results shows, that thermal overheating effects even under normal operation voltages have a strong influence on HEMTs characteristics. The observed saturation of current trough TLM structure confirms that both thermal overheating and hot electron effects are playing role in the current reduction. We developed a theoretical model which allow to discriminate between the current reduction caused by increasing electric field and channel temperature rise due to the self-heating. The microsecond pulse measurements shows 60% reduction of self-heating compared to DC measurements, in agreement with our calculations. The results obtained allow us to suggest that to utilize unique properties of group III-nitride heterostructures, including high speed of the electrons, it is necessary to optimize the thermal budget of devices.

2.2 Two-dimensional electron dynamics under low and high electric field.

Being very perspective materials for applications in high power and high temperature electronics III-V nitride based materials represent by itself *terra incognita* in some fields [31]. Particularly, high-field transport properties of nitride materials are not studied in detail. These include: mechanisms of relaxation of hot carrier, intervalley transfer, the velocity-field characteristics, etc. Up to date there are no experimental measurements of the velocity-field characteristics in two-dimensional III-V nitride based heterostructures at the electric fields close to the critical one in this material system. This information on the hot carriers is of the fundamental importance for the performance of all semiconductor electronic devices.

High electric currents and fields, which are characteristic for the nitrides, give rise to ultra-high dissipative power and considerable Joule heating of the samples [38]. As we have seen from results of the previous chapter, nanosecond pulses are required if we want to remove self-heating and measure only hot-electron effects. In this section we present experimental results on of the velocity-field characteristics in AlGaN/GaN heterostructures obtained by using 10 ns-pulse current-voltage measurements.

2.2.1 Structure design and experimental setup

The investigated devices were fabricated from $Al_{0.33}Ga_{0.67}N/GaN$ undoped heterostructures of 1.1 μm GaN and 23 nm AlGaN covered with a 320 nm Si_3N_4 passivation layer. The structures were grown by metal organic chemical vapour deposition (MOCVD) on sapphire substrates with 40 nm $Al_{0.16}Ga_{0.84}N$ intermediate nucleation layer. The transmission line model (TLM) patterns of different lengths L of conduction channel and equal width W were studied. The channel length varied from 1 to 35 μm, while the width was 100 μm. The TLM ohmic contacts were processed by Ti/Al/Ti/Au metallization annealed for 40 s at 800^0C.

The high field experiments, particularly the current-voltage characteristic measurements, were carried out by using of nanosecond voltage pulses applied to the sample. This pulse regime minimizes the self-heating effects. The measurements were performed in a temperature range between 4.2 K to 300 K. The electric pulses were generated by discharging of coaxial line through a mercury-wetted relay. The coaxial line was charged by a DC voltage source, this method allows us to obtain the electric pulses of 10-30 ns duration of different magnitudes.

The used electric circuit is shown in Fig. 2.6 (a). The resistor module comprised 80 Ohm loading resistor in parallel with the sample and 50 Ohm resistor for a current control. It was found that the sample resistance increased from 30-50 Ohm at low fields up to 400-500 Ohm at the high fields of 100-150 kV/cm. This effect gives rise to changes in pulse reflection during the experiments. The 80 Ohm resistor provides minimization of the load mismatch altered with electric pulse magnitude. A two-channel stroboscopic oscilloscope with 0.1 ns resolution allowed measuring the applied voltage in point B and voltage on 50 Ohm resistor in point A, both points are indicated in Fig. 2.6 (a). The pulse measurements were carried out in a helium cryostat: at 4.2K the sample was immersed into the liquid helium, while at elevated temperatures (up to 300 K) the helium gas flow was used for better electrical isolation. The typical waveforms of the current and the applied electric voltage pulse are shown in Fig. 2.6 (b). The waveform coincidence of the both signals was observed at all temperatures of the experiment and it did not alter with electric pulse magnitude.

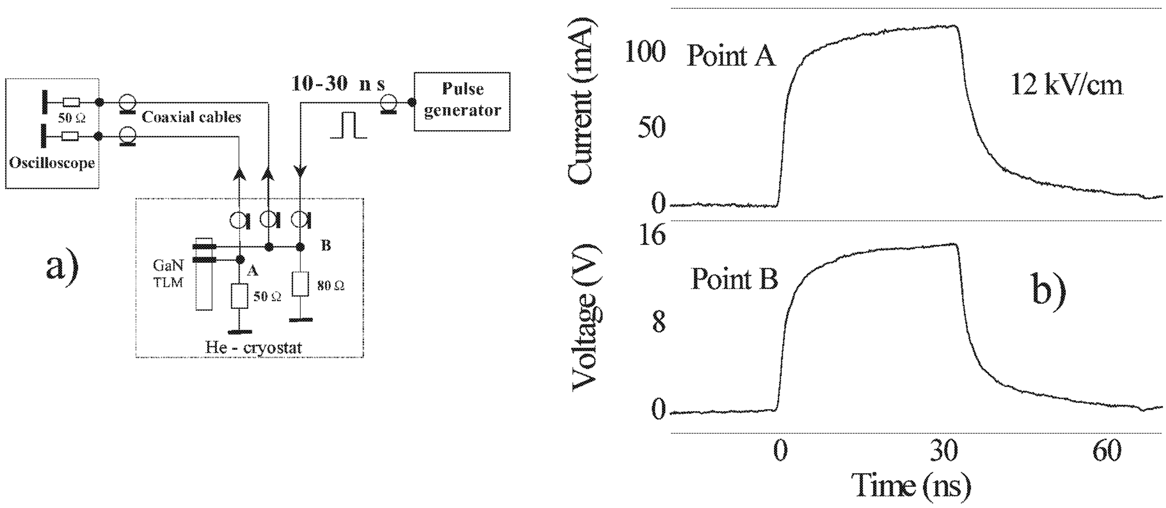

Figure 2.6. (a): Experimental setup for pulse measurements. (b): Current and voltage waveforms measured at points A and B marked in Fig. 2.6 (a).

2.2.2 Low-field investigation of 2DEG

Firstly we conducted the low-field measurements to determine basic parameters of 2DEG. By applying the Van der Pauw method we found that the low field mobility equals 4000 $cm^2/V\,s$ at 4.2 K and 1250 $cm^2/V\,s$ at 300 K. The measured temperature dependence of the mobility is presented in Fig. 2.7. For the sheet electron concentration we found $n=1.05\text{x}10^{13}$ cm^{-2} in the measured temperature range (1.4- 400 K). We also conducted magnetotransport measurements. The strong Shubnikov-de Haas (SdH) oscillations are observed, as illustrated by the inset to Fig. 2.7. The SdH oscillations appeared at relatively low magnetic fields, which is evidence for good quality of the AlGaN/GaN heterointerface. The sheet carrier concentration determined from the SdH oscillations was nearly the same as the one yielded by the Van der Pauw method.

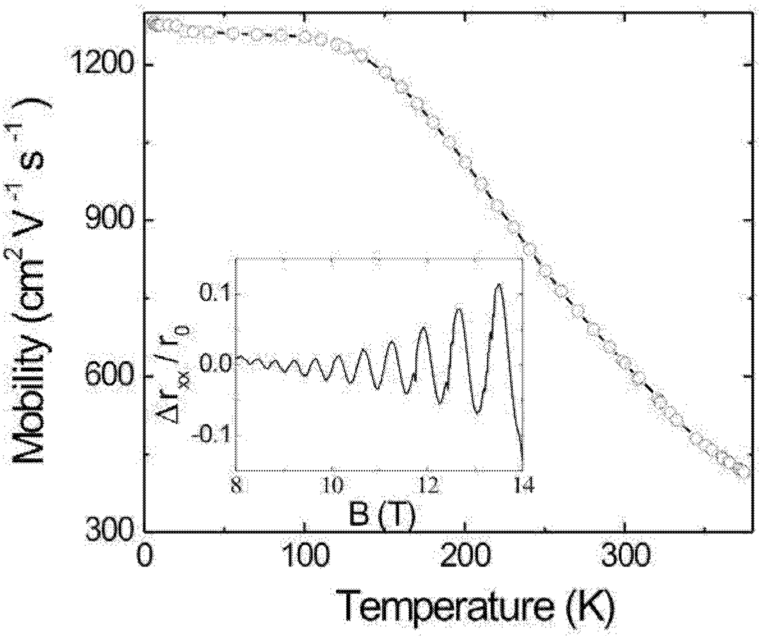

Figure 2.7. Electron mobility versus ambient temperature. In the inset: the SdH oscillations at T = 1.4K.

It is interesting to note that the magnetotransport measurements shed a light on mechanisms of low field scattering of electrons. From the Dingle plot (Fig. 2.8)of the SdH oscillations amplitude as a function of reciprocal magnetic field we estimated the so-called "quantum scattering time".

The quantum scattering time, τ_q, is related to the Landau level broadening and characterizes the total carrier scattering mechanisms. A simple equation can be used [39]:

$$\ln[\frac{\Delta\rho_{xx}}{\rho_0 D_T}] = C - \frac{\pi m^*}{e\tau_q}\frac{1}{B}, \qquad (1.4)$$

where $D_T = \frac{4X}{\sinh X}$, $X = \frac{2\pi^2 kT}{\hbar\omega_c}$, $\Delta\rho_{xx}$ is the amplitude of the oscillations, ρ_0 is the zero-field resistivity , ω_c is the cyclotron frequency, e is the electron charge, m^* is effective mass, B is magnetic field, C is constant at a given temperature, $\hbar$ is reduced Plank's constant, k is Boltzmann's constant, T is temperature.

By fitting the data plotted in inset of Fig.2.8 and taking the electron effective mass m^* as $0.23m_e$, we obtain that the quantum scattering time is 61.8 fs. The latter corresponds to broadening value of the Landau level of 2.86 meV.

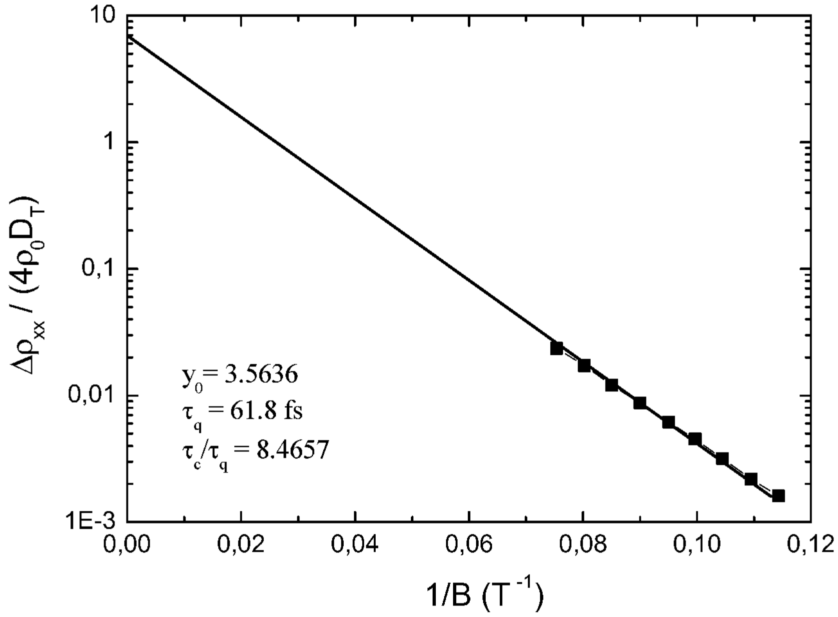

Figure 1.8. Dingle plot of SdH oscillations amplitude vs the reciprocal magnetic field.

Classical transport time, τ_t, derived from the low-field mobility is 0.53 ps. The relation between two times is a characteristic of the dominant angle of scattering events in the 2DEG. For short-range scattering process on roughness and imperfections of the heterointerface large angle scattering events will be dominant and the ratio is expected to be unity. It will be several times higher then unity in the case of long-range/small angle scattering processes.

The average ratio of the ”classical” transport time found from the measured mobility to the ”quantum time” was found to be around 8. For comparison the highest value observed in high-mobility modulation-doped AlGaAs/GaAs 2DEG where small angle scattering processes are dominant is 30 [40]. The fact is consistent with reduced defect scattering of 2DEG formed at interface between undoped layers. This also consists with our results of low frequency noise measurements, which ones yield the value of Hooge parameter comparative with GaAs structures, as it will be shown in Chapter 3. The low value of magnetic field at which the SdH oscillations are resolved is also characteristic of small disorder at AlGaN/GaN interface.

2.2.2 High-field electron dynamics

The typical results of high-filed measurements of the current are illustrated in Fig. 2.9, where the current-voltage characteristics are presented for two samples with L = 5 μm and L = 10 μm at different ambient temperatures. General features of these results are: a rapid increase in the current from 0 to 0.15 A at low voltage bias (< 10 V) and an extended portion with a slow increase in the current at larger biases. Slightly higher currents occur at lower ambient temperature. Currents of 1.5 A/mm are achieved at high voltages. These values are larger by one order of magnitude than the currents observed in HFET and MOSHFET-nitride structures [41]. These values can be explained by the absence of the gate leakage currents. Note that the studied two-terminal devices can be used for limitation of current for electrical pulses of 10 ns duration.

To determine the electron drift velocity we used the relation

$$V_{dr} = I/enW, \qquad (2.5)$$

where I is the current, e is the electron charge, n is the carrier concentration. This method of determination of V_{dr} relies on the measured value of the electron concentrations and on the assumption that the concentration remains constant as the electric field changes.

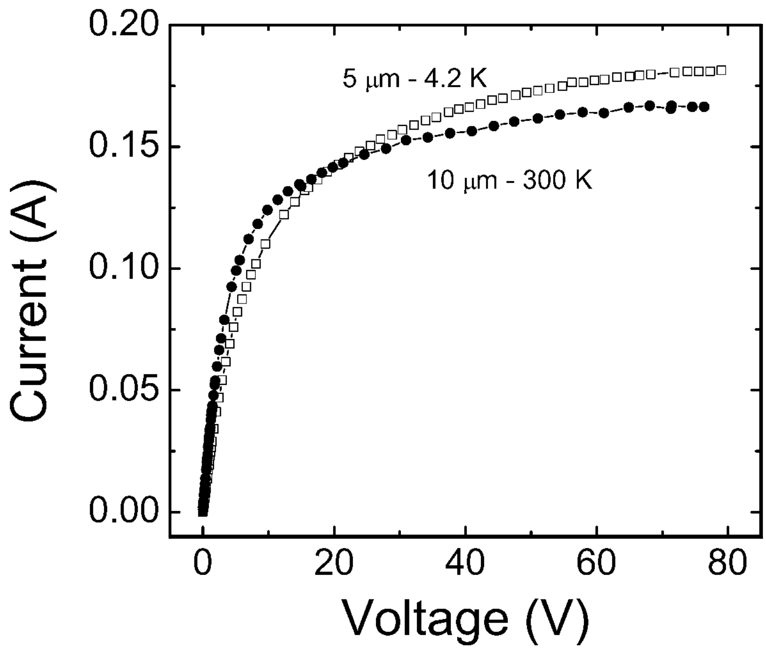

Figure 2.9. Current-voltage characteristics for two TLM samples. Open symbols correspond to L =5μm, T =4.2K, solid symbols correspond to L = 10μm, T = 300K.

Calculated with equation (2.5) V_{dr} -E curves are shown in Fig. 2.10. The curves measured on TLM with different length are very similar. A linear increase in the velocity up to the electric fields of about 5 kV/cm is followed by sub-linear dependence for both presented samples. Remarkable, that despite our nitride structures have relatively small low-field electron mobility (4000 and 1250 cm^2/Vs at 4 K and 300 K, respectively) we obtain the magnitude of the drift velocity above 10^7 cm/s. Together with large electron concentrations this produce high current densities (I =2.5 A/mm) and record specific input electric power (~100 W/mm).

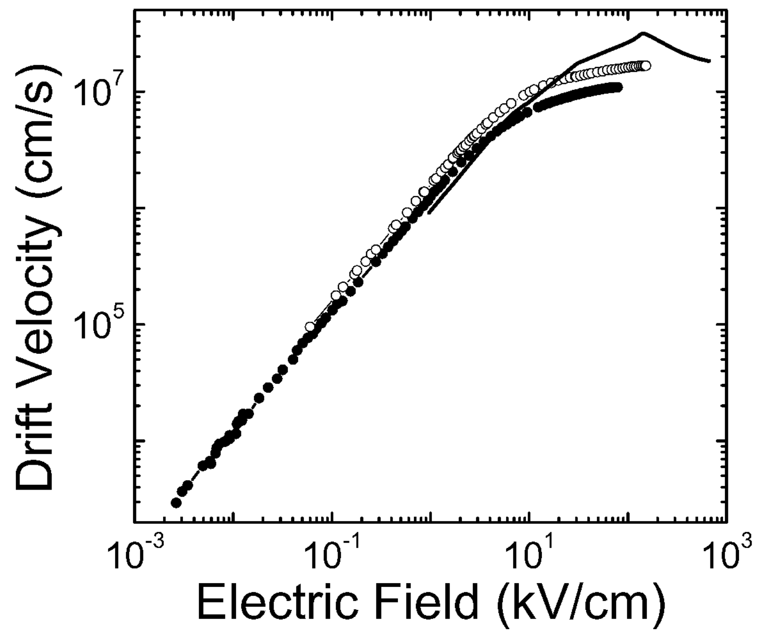

Figure 2.10. Electron velocity versus electric field for the same samples and temperatures as in the Fig. 2.9; solid curve represents the theoretical dependence.

The maximum of achieved drift velocity equals 1.7×10^7 cm/s at E = 150 kV /cm (T =4 K) and 1.1×10^7 cm/s at E = 80 kV /cm (T = 300 K). These magnitudes of V_{dr} obtained for the 30 ns electric pulses are larger than those we measured for the longer pulses. The found velocity magnitudes are close to the values V_{dr} measured for the perfect modulation doped AlGaAs/GaAs structures. Indeed, for lightly doped AlGaAs/GaAs structures (n=4×10^{11} cm^{-2}) with mobility 7600 $cm^2/V\,s$ at T = 300 K, it has been found that $V_{dr} \leq 1.7\times 10^7$ cm/s [42].

For another relevant analysis, we compared the $V_{dr}(E)$-dependence with theoretical curve, calculated in the model of the shifted Maxwellian distribution taking into account known scattering mechanisms, particularly electron-optical phonon interaction. In Fig. 2.10 these results are shown for the ambient temperature 300 K. The theoretical values are slightly larger than the measured ones. This can be explained by the fact that for the 30 ns electric pulses Joule heating still exists. Estimates show that a decrease in the pulse duration to 1- 2 ns should lead to higher velocity.

Now we shall discuss the electron temperatures T_e in the nitride samples. For moderate electric fields, when the drift velocity is small in comparison to the thermal electron velocity ($V_{dr} << \sqrt{2k_B T_e / m}$, k_B and m are the Boltzmann constant and the effective mass, respectively), the electron temperature can be estimated by the "mobility comparison" method [43]. This method consists in the measurement of the low-field mobility at different ambient temperatures $\mu(T)$ and the measurement of the hot-electron mobility as a function of the electric field $\mu_{he}(E)$. Since the distribution function of the electrons can be described by the Maxwellian function with substitution $T \rightarrow T_e$, equating the found dependences $\mu(T_e) = \mu_{he}(E)$ one can estimate the function $T_e(E)$. We used the results presented in Fig. 2.7 on $\mu(T)$ in the interval 4.2-350 K to determine $T_e(E)$-dependence for the field range 0-15 kV/cm, as presented in Fig. 2.11 (a). By using this dependence, one can calculate dissipated electrical power per electron P_e as a function of $1/T_e$. The corresponding data is shown in Fig. 2.11 (b). The high temperature portion of these data (200 K < T < 350 K) can be described with the energy relaxation rate via optical phonon emission equation:

$$P_e = \frac{\varepsilon_0}{\tau_0} \exp(\frac{\varepsilon_0}{kT_e}), \qquad (1.6)$$

where ε_0 is the optical phonon energy and τ_0 is the characteristic time of optical phonon emission.

This equation agrees well with the data presented in the inset for the parameters ε_0= 92 meV and τ_0 = 25 fs. Remarkably, the latter value can be calculated via the Frölich coupling constant α: $\tau_0 = h/(2\alpha\varepsilon_0)$. For GaN parameters[31],[44] we calculated α = 0.41 and τ_0= 20 fs, i.e., both estimates coincide very well.

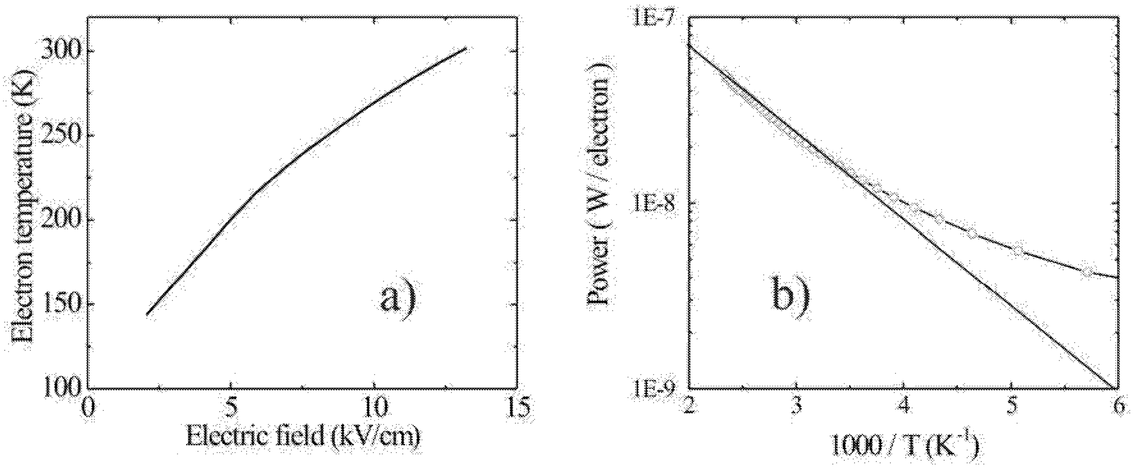

Figure 2.11. (a): Estimated electron temperature versus electric field. (b) Dissipated power as a function of inverse electron temperature.

In conclusion, by applying 10-30 n*s* electrical pulses to AlGaN/GaN gateless heterostructures, we experimentally measured low field and high field transport phenomena, including the drift velocity dependence on the applied electric field up to record high 150 kV/cm. Particularly, the current density in excess of 1.5 A/mm was measured at high voltages. These values are higher by one order of magnitude in comparison with the currents observed in gated nitride structures. For the measured samples with the high electron concentrations, the electron distribution function is determined by the shifted Maxwellian distribution with two parameters: the electron temperature and the drift velocity. It is remarkable, that despite the measured nitride structures have moderate values of the low-field electron mobility we obtained a drift velocity of 1.7×10^7 cm/s at the field 150 kV/cm. This magnitude is still lower than the theoretical limit (~3×10^7 cm/s). However it is very close to the values V_{dr} measured for the perfect modulation doped AlGaAs/GaAs structures.

Chapter 3: Properties of *1/f* noise in AlGaN/GaN heterostructures

Besides the self-heating, another strong limitation of high frequency devices is low-frequency noise. Microwave transistors designed on the basis of AlGaN/GaN heterostructures demand intensive investigations in order to optimize the material characteristics to attain high power and low-noise operation. Today, GaN-based High Electron Mobility Transistors (HEMTs) possess still comparatively high level of leakage current due to large dislocation density and material layers imperfections [45,46,47]. The inhomogeneities arise due to either growth technique and/or the device design technology. As a result, the current fluctuations originate from contributions of different sources distributed throughout the semiconductor structure used in the device fabrication. Thus, investigation of the noise sources is very important to identify the output noise as well as to control its level. In this chapter, we address the study of excess low-frequency *1/f* noise sources in Group-III nitride-based (AlGaN/GaN) high electron mobility transistors (HEMTs) grown on sapphire. The devices are scaled down to nanometer range with the gate length of 150, 250, and 300 nm, in contrast to previous studied devices with gate length of a micrometer range scale [48]. It will be shown, that devices with a shorter gate length show new features of the carrier transport and noise, which impact appreciably the device performance.

3.1 The study of low-frequency noise peculiarities of the AlGaN/GaN HEMTs.

In spite of continuous progress in growth technology of GaN-based structures and very promising results for their high power and high frequency applications further investigation of native defect structure as well as search of new ways for improvement of material characteristics are necessary. Investigation of low frequency noise is one of the methods for characterisation of material quality and a number reports were devoted to the analysis of *1/f* noise in AlGaN/GaN high electron mobility transistors (HEMT) [49],[50]. Nevertheless, the mechanism of the low frequency noise in GaN-based devices has not been understood yet. In particular, the reasons for deviations from *1/f* law should be clarified.

3.1.1 Transistor fabrication and experimental details

AlGaN/GaN HEMTs under investigation were grown by metalorganic chemical vapor deposition on sapphire substrates. A 40 nm AlGaN (16% Al) nucleation layer grown on the substrate was followed by the deposition of a 1.1 μm nominally undoped GaN buffer layer and a 23 nm AlGaN (33% Al) undoped barrier layer. Transistors were fabricated using Ti/Al/Ti/Au metallization annealed for 40s at 800^0C for source and drain ohmic contacts and Ni/Au for Schottky gate contacts. The surface was covered with 320 nm Si_3N_4. The devices had gate length of 0.15, 0.25, 0.30, 0.35 μm, gate width of 100-400 μm, and drain-gate spacing of 1 μm. Source-drain spacing was of 3 μm. A complete direct current characterization has been carried out in HEMT devices with variety of channel's width and length. Hall mobility and sheet carrier concentration in ungated structures were extracted from Hall measurements. A room temperature electron mobility of 1250 cm^2/Vs at a sheet carrier density of $1.05\times10^{13}cm^{-2}$ was measured in the channel.

Transistor's DC characteristics were investigated with an HP4145B semiconductor parameter analyzer operated in transistor mode.

Low-frequency noise measurements were performed at different gate-source voltages in the common source configuration under open circuit conditions $R_L >> r_d$, where R_L is the load resistance in the drain circuit and r_d is the channel differential resistance. The noise spectra were measured in the frequency range from 1 Hz to 100 kHz at 300 K with using low-noise preamplifier ITHACO 1201. The directly measured noise power density $S_{Vm}(f)$ was analyzed by HP35670A Dynamic Signal Analyzer.

Then the noise spectra of the transistors were obtained by:

$$S_V(f) = \left[\frac{S_{Vm}(f)}{G^2} - S_{Vb}\right] \Big/ k(f), \tag{3.1}$$

where $S_{Vb}(f)$ is the background noise of the low-noise preamplifier, G and $k(f)$ are the preamplifier's gain and a correction factor to a nonuniformity of the gain frequency behaviour (normalized amplitude-frequency characteristic), respectively. We used a set of wire load resistors RL that did not contribute an additional excess noise.

3.1.2 DC measurements results

The DC current-voltage (I-V) characteristics (Fig. 3.1) of the 150 nm HEMT were obtained for different gate voltages from 0V to –5 V.

It is seen that the I-V curves can be divided into two groups which are discriminated by a threshold value of the gate bias V_{Gt} = -3 V (dashed line in Fig.2.1) , for $V_G \geq V_{Gt}$ and for $V_G < V_{Gt}$. The former, corresponding to the low gate voltage measurements, is characterized by very weak deviation from linear behavior (even at a relatively high drain-source voltage of $V_D \approx 2$ V) and a weak dependence on the gate bias. On the contrary, the latter corresponds to the transistor operation practically in subsaturation regime at such gate biases, so that only initial part of the I-V curves ($V_D \leq 150$ mV) is linear. Thereby, $V_G = V_{Gt}$ is the threshold gate bias which distinguishes different regimes of the transistor operation with weak and strong control of the channel resistance.

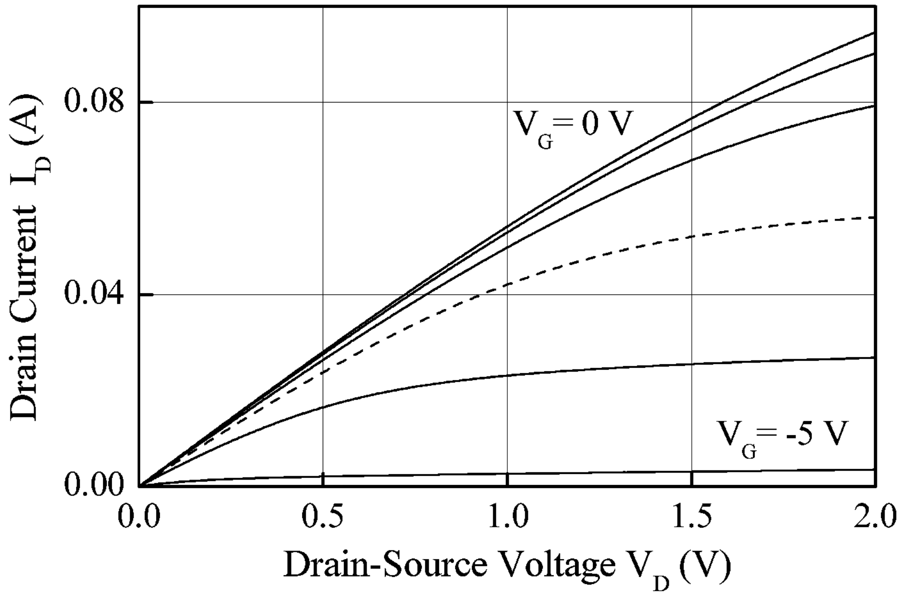

Figure 3.1. The DC I-V characteristics of the transistor measured for different gate voltage V_G from 0 to –5 V with step –1 V.

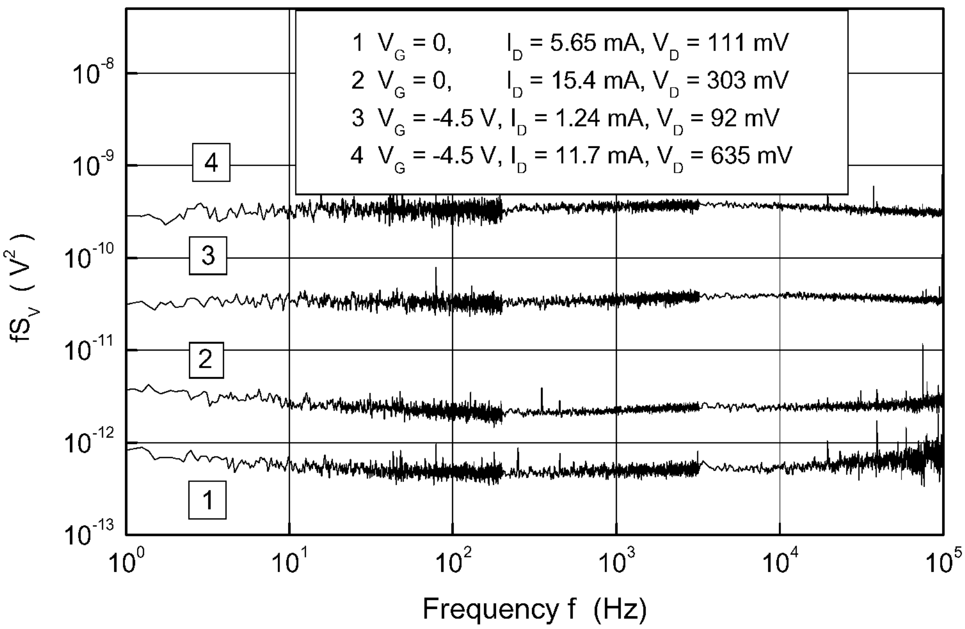

Figure 3.2. Normalized frequency spectra of the voltage noise at certain gate biases below (curves 1,2) and above (curves 3,4) the threshold voltage V_{Gt}: 1 - V_G = 0 V; I_D = 5.65 mA; V_D = 111 mV; 2 - V_G = 0 V; I_D = 15.4 mA; V_D = 303 mV; 3 - V_G = -4.5 V; I_D = 1.24 mA; V_D = 92mV; 4 - V_G = -4.5 V; I_D = 11.7 mA; V_D = 635 mV.

3.1.3 Low-frequency noise measurements results

The voltage-noise spectral density $S_V\,(f)$ was obtained for different gate voltages in the range of 0 -5 *V* and for drain currents in the range of 1 – 26 *mA*. The spectra show frequency dependence of the type of $1=f^{\gamma}$ with the exponent γ being very close to unity (*1/f* noise). The background noise of preamplifier became apparent only for relatively small noise levels at the very high frequencies used in the experiment, which will be beyond of our considerations. The gate voltage of about -3 *V* has been found to discriminate the noise spectra behaviour for both the frequency dependence and the drain-source current dependence at a given frequency of the analysis. In Fig. 3.2, we show two groups of the normalized spectra of the drain-source voltage noise at different gate biases, $V_G > -3$ *V* (curves 1,2) and $V_G < -3$ *V* (curves 3,4). Within each group of curves the gate voltage is the same whereas the drain current is different. The spectra shape does not depend on the drain current, while it is changed with the gate bias. For the first group of measurements, an increase in the noise spectral power $S_V\,(f)$ is observed (with respect to the *1/f*-dependence) at the very low frequencies, as well as somewhat elevated values of high-frequency contributions. In the spectra of the second group, the low-frequency growth is not observed and there is a maximum at frequencies of 3–10 *kHz* dependent on the source-drain voltage. These peculiarities in the noise spectra may be due to the occurrence of local levels with distinct characteristic time constants, which need further investigation.

For the analysis of main contributions to the observed noise, we study the dependences of the drain current-noise spectral density $S_I(f) = S_V\,(f)/r_d^2$ on the drain current I_D for different gate biases and for a given frequency f = 10 Hz (Fig. 3.3). It is remarkable that the same value of the gate bias, V_{Gt}, obtained for the DC current-voltage characteristics, determines in Fig. 3.3 two regions where the noise level is weakly and strongly controlled with the gate voltage. The studies of the origin of the low-frequency noise in field-effect transistors are performed usually in linear regime of operation. We analyze the results of the noise measurements relevant to this regime (-4.5 V ≤ V_G ≤ 0 V and V_D ≤150mV (Fig. 3.1)), considering the two groups of curves distinguished in Figs. 3.1 and 3.3.

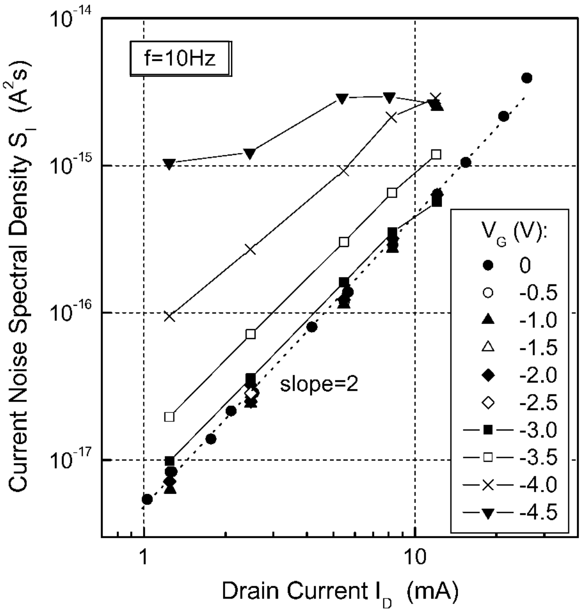

Figure 3.3. Dependences of current-noise spectral density on the drain current I_D measured at frequency f = 10Hz and different gate biases V_G from 0 V to -4.5 V; the dotted curve shows the quadratic dependence of S_I vs I_D.

Concerning the first group of measurements (-3 V $\le V_G \le$ 0 V), it is to be noted that differential resistance of the channel is varied only weakly, $r_d \approx 20\ \Omega$ for $V_D \le$ 150mV (Fig. 3.1), and the noise level practically is not changed with the gate voltage (Fig. 3.3). The dependence of S_I on I_D is strictly quadratic. This proves that the measured noise is not a contact one but caused by fluctuations of the channel resistance. It is usually characterized by the so called Hooge parameter α_H, dimensionless measure of a "noisiness" of the structure:[18]

$$\alpha_H = \frac{S_I(f)}{I_D^{\ 2}} f N , \qquad (3.2)$$

where N is the total number of the conduction electrons in the noise region.

Expressing N as $\frac{L^2}{q\mu_n R}$, and taking into account that $I_D^2 = \frac{V_D^2}{R^2}$, equation (3.2) can be transformed to:

$$\alpha_H = \frac{S_I(f)}{V_D^2}\left(f L^2 R / q\mu_n\right), \qquad (3.3)$$

where L is the channel length, R - is the channel (ohmic) resistance, μ_n is the electron mobility, and q is the electron charge.

Using the data of Figs. 3.1 and 3.3, the Hooge parameter was calculated by Eq. (3.3) at $V_G = 0$ V, $V_D = 100\ mV$, $I_D = 5\ mA$, and $L = 0.15\ \mu m$ is as low as $\alpha_H = 2.7 \times 10^{-6}$, which is an incredibly small quantity. Such a discrepancy can be eliminated if we take that the device noise for the considered range of gate biases (in the linear regime of operation) is determined by the noise sources located in passive (ungated) regions adjacent to the drain and source contacts (Fig. 3.4). In this regime, the resistance of the active (gated) region is a small part of the total resistance of the transistor channel between the drain and source contacts.

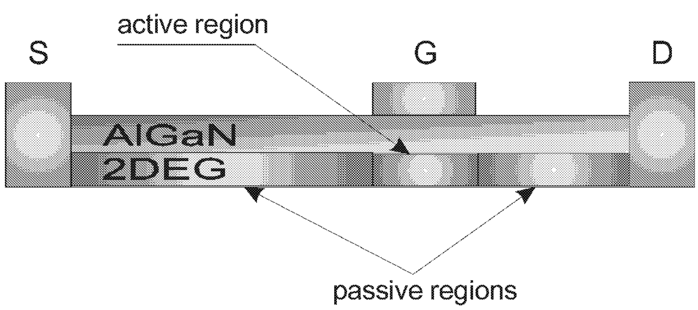

Figure 3.4. Schematic description of the structure under investigation with active and passive regions of the channel defined.

Indeed, if we use in Eq. (2.2) the distance L = 3 μm, then we obtain $\alpha_H = 10^{-3}$. This value of α_H is comparable to the standard magnitude [29] of $\alpha_H = 2 \times 10^{-3}$, as well as to that previously obtained for nitride heterostructures grown on sapphire substrates [51],[52],[53].

The second group of curves in Fig. 3.3 ($V_G < -3\ V$) is characterized by a lower slope of the dependence $S_I(I_D)$, with the slope being decreased with increasing the gate bias. Moreover, the noise spectral level S_I for this group of measurements exceeds the respective values of S_I for the first group of curves discussed above. Such a distinct separation in the behaviours of the spectral noise density $S_I(I_D)$ at $V_G = -3\ V$ allows to distinguish between noise coming from passive ($\alpha_H = \alpha_H^p$) and active ($\alpha_H = \alpha_H^a$) regions of the transistor channel. Assuming uncorrelated noise contributions from different regions, the voltage noise of active region, S_V^a, can be determined by subtracting the noise of passive region, S_V^p, from the total noise power $S_V = S_V^p + S_V^a$, that has been measured in the experiment under given DC current regime. The DC and noise performance of the passive region can be determined from experimental results corresponding to zero gate bias, i.e., we take the resistance of the passive region to be $R_p = (V_D/I_D)|_{V_G=0}$ and the respective voltage-noise spectral density to be $S_V^p = S_V(V_G = 0)$. Respectively, for the active region we can write $S_I^a = S_V^a/(r_d^a)^2$, where differential resistance of the active region is just its ohmic resistance $r_d^a = V_D^a/I_D$ (linear regime), and $V_D^a = V_D - I_D R_p$ is the voltage drop across the active region. Thus, the Hooge parameter attributed to the active region of the transistor channel can be calculated by:

$$\alpha_H^a(V_G) = \frac{S_I^a(f, V_G)}{(V_D^a)^2}\left(f L_a^2 R_a / q\mu_n\right) \qquad (3.4)$$

Here, we have assumed the electron mobility to be the same all over the passive and active regions. From Eq. (3.4), the value of the Hooge parameter has been extracted, $\alpha_H^a \cong 2\times10^{-4}$. It is found for the investigated transistors that α_H^a is independent on the gate bias in the range of $-4.5\ V \leq V_G \leq -3\ V$.

Thus, a Hooge parameter has been extracted separately for passive α_H^p = 10^{-4} - 10^{-3} and active α_H^a = (1-2)x10^{-4} regions, respectively. One of possible reasons for a decreased Hooge parameter can be strong Coulomb correlations between the channel and trapped to localized states electrons considered in [54].

The experiments carried out reveal also strong correlation between leakage currents and the noise spectra. In particular, deviation from *1/f* dependence is observed in the structures possessed a low level of leakage currents (Fig. 3.5). It is seen from Fig.3.5 that deviation from *1/f* dependence occurs in extended range of frequency and one becomes more pronounced with increase of gate voltage.

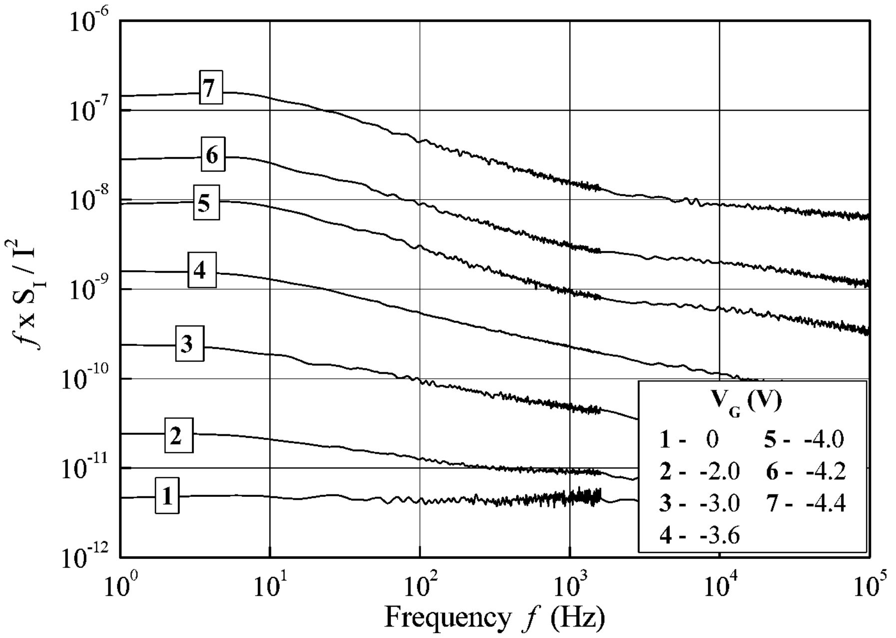

Figure 3.5. Normalized frequency spectra of the current noise of the transistor with low leakage current at certain gate biases.

The observed peculiarities in *1/f* noise spectra have been exhibited most distinctly in gateless devices, in particular, the transmission line model (TLM) patterns. A distinctive feature of the noise in TLM structures is that the deviation from *1/f* law is observed at high enough voltages only. Moreover, the magnitude of the deviation increases monotonously with applied voltage approaching the saturation at bias voltage $V > 6$ V. The slope in logarithmic scale of the transition region observed in the noise spectra (Fig. 3.5) changes also. It increases from 1 at bias voltage $V < 0.1$ V up to 2 at $V > 6$ V. The behaviour observed cannot be explained by conventional generation-recombination processes [55]. In our opinion, a model based on dynamic redistribution of potential along the channel is more relevant. Static approach to such redistribution has been developed in [56].

The essence of the model presented in [56] is as follows. Let consider the existence of an additional conductive channel located either on the surface or in the barrier layer at small distance from the basic 2DEG channel. A strong electrostatic coupling between the 2DEG and additional channels arises. As a result at high enough applied voltage the difference in lateral distribution of the potential in the basic and additional channels leads to redistribution of charge in the additional channel. The latter should stipulate redistribution of the transverse potential that supports 2DEG in the basic channel. Finally, lateral distribution of electron density in the basic channel is changed. In our model inherent density fluctuations in the 2DEG play the role of dynamic inhomogeneities. These fluctuations being connected with electrons in the additional channel pull them along. Due to this effect at low frequency slow electrons of the additional channel contribute to *1/f* noise together with fast electrons of the basic channel that causes increase of *1/f* noise level. At high frequency slow electrons of the additional channel cannot response to fast fluctuations of the 2DEG. In this case there is no extra contribution to the *1/f* noise.

The model suggested is confirmed by the experiment. The noise spectra of ungated TLM structures measured at 300 K are presented in Fig. 3.6. The background level is shown by dotted lines. According to our model this level corresponds to initial noise (*1/f* noise level of the 2DEG only).

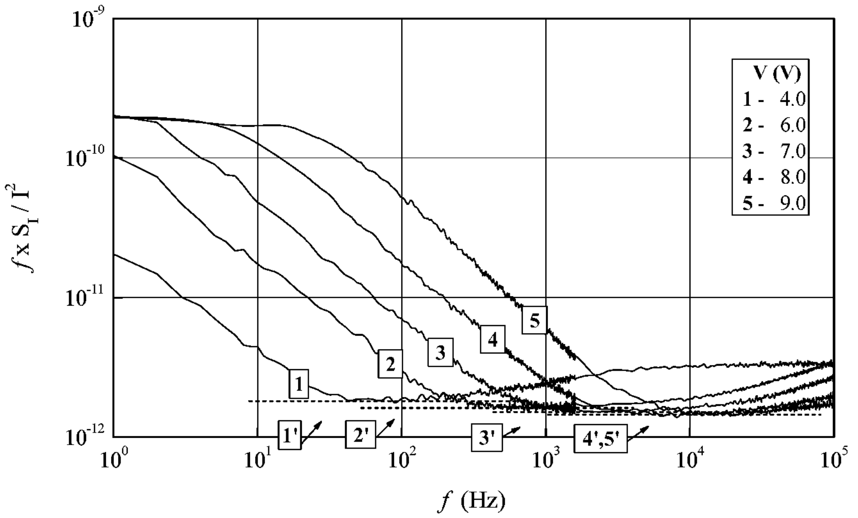

Figure 3.6. Normalized frequency spectra of the current noise of the TLM pattern at certain bias voltages.

To study fine structure of the spectra shown in Fig. 3.6, we subtracted the background noise level from the total one. The result is depicted in Fig. 3.7. Analysing the curves in this figure we can conclude that low-frequency part of the spectrum and *1/f* region corresponding to minimal value of the $(f\,S_I/I^2)$ quantity are not additive [55], but they are components of the complex noise spectrum. In other words, they are correlated.

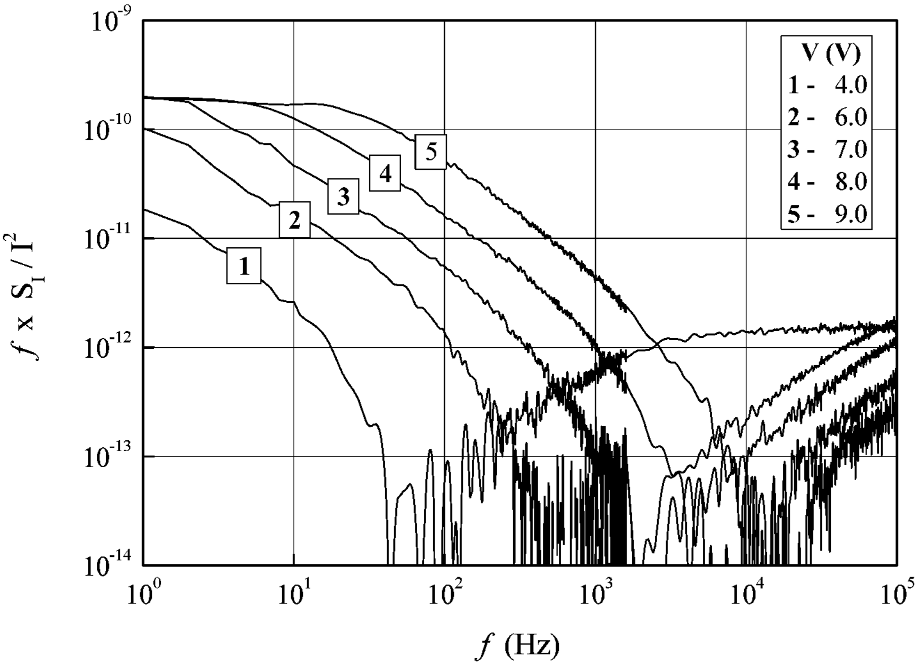

Figure 3.7. Noise spectra presented in Fig. 3 after subtraction of the background noise.

The latter confirms the above mentioned statement that low-frequency rise of the noise level represents by itself transformed initial *1/f*-fluctuations, but not a separate, additional noise, e.g., generation-recombination (GR) noise. It should be noted that in high-frequency range of the spectra shown in Fig. 3.7 there are regions with the slope equal to 1 in logarithmic scale that is, obviously, manifestation of the GR fluctuations additive to *1/f* ones.

Another testimony of the fact that *1/f* regions corresponding to minimal value of the (fS_I/I^2) (Fig. 3.6) are spectra of initial *1/f*-fluctuations is presented in Fig. 3.8.

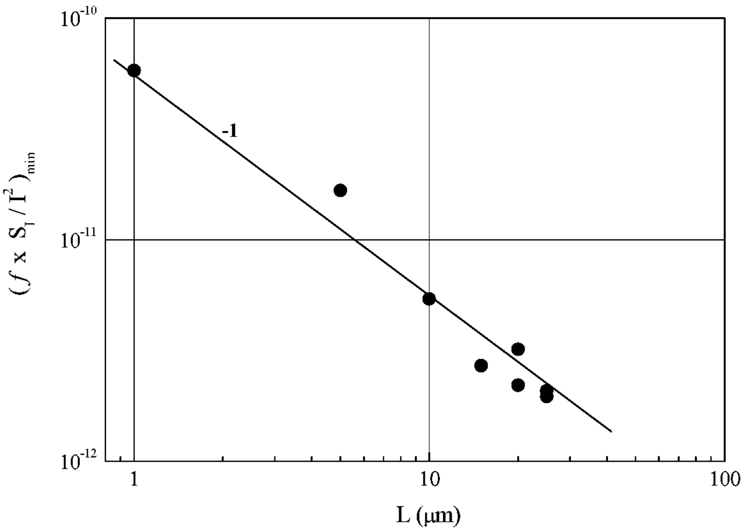

Figure 3.8. Dependence of the background noise on the length of the 2DEG channel.

It is clearly seen that reciprocal dependence of $(fS_I/I^2)_{\min}$ on the channel length, L, is in a good agreement with Hooge's law for *1/f* noise:

$$\frac{f \cdot S_I}{I^2} = \frac{\alpha_H}{N} \sim \frac{\alpha_H}{L}, \tag{3.5}$$

where S_I is the current-noise spectral density, and I, f, α_H, N are the current, frequency, the Hooge parameter, and the number of charge carriers, respectively. It means that minimal value of the (fS_I/I^2) indeed corresponds to the level of initial *1/f* noise.

However, we cannot state precisely, that our noise is governed completely by Hooge model. Another popular *1/f* noise theory of McWorter also can be applied here. The difference between these theories is very difficult to distinguish experimentally and can be determined only for some special cases. For our TLM structures case, as objects of investigation both the McWorter and Hooge models lead to a $\frac{fS_I}{I^2} \sim \frac{1}{L}$ dependence of normalized noise on the sample length. Such dependence is confirmed by our measurements (see Fig. 3.8) and is in good agreement with both theories.

A characteristic quantity of the effect under study is time constant of the noise transformation process, τ_0, that corresponds to frequency of transition from *1/f* dependence to a more strong one (transient frequency). Upon the lowering temperature the transient frequency shifts towards low frequencies and exhibits an exponential dependence on temperature with an activation energy of 0.4 eV (Fig.3.9). In McWorter's model the origin of *1/f* noise is considered to be caused by uniformly distributed traps in space and energy [57]. Therefore, any deviation from *1/f* dependence can be explained as a result of non-uniform distribution of noise sources. However, the exponential temperature dependence of the frequency shift is not inherent in the McWorter *1/f* noise. Thus, McWorter's model alone cannot explain the features observed in the spectra with decreasing temperature and should be supplemented to describe the observed features.

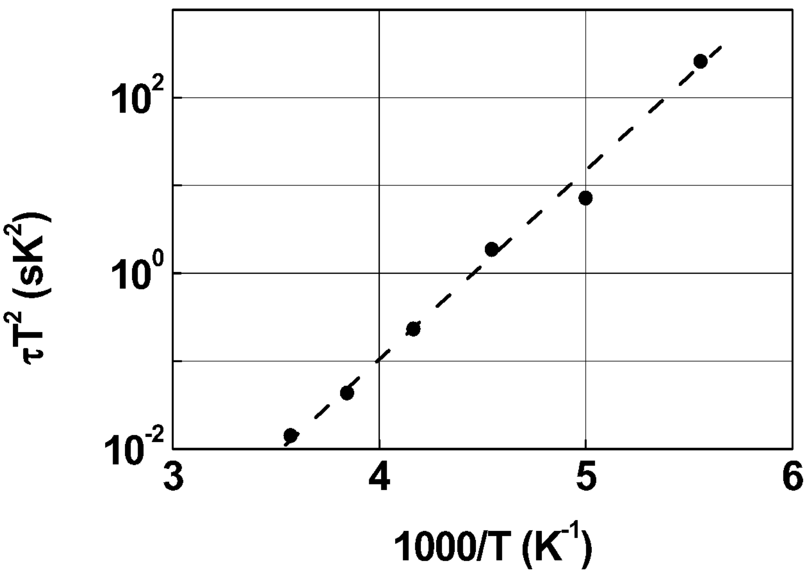

Figure 3.9. Inverse temperature dependence of the normalized transient time (Arrhenius plot). Dashed line corresponds to linear fit with the activation energy level of 0.4 eV.

We suggest the following model of the origin of flicker (*1/f*) noise at low temperatures. The exchange by electrons between 2DEG and traps located in the barrier layer occurs due to tunnelling as in McWorter's model accompanied simultaneously by an additional activation process. The fact that a minimum noise level exists in the *1/f* spectra at low frequencies argues in favour of the model. The noise level does not depend on temperature and this therefore demonstrates that its origin is due to tunnelling.

In conclusion, an adequate method for the low-frequency noise sources characterisation from different device regions is proposed and tested for nanoscale Group-III-nitride heterostructures. The revealed behaviour of the noise spectra as well as the small value of the Hooge parameter is discussed within theoretical models of the noise associated with the specific resistance fluctuations. Temperature dependence of the noise revealed characteristic frequency of transition from *1/f* dependence to a stronger one. The process has activation energy of 0.4 eV, which can be related to the traps in AlGaN barrier.

3.2 Noise properties of barrier layer of GaN-based HEMTs

Another noise that is especially important for HEMTs, operating in high frequency regimes is the noise of current trough the barrier layer. The problem whether the measured noise of a field effect transistor (FET) is the channel noise or it is manifestation of leakage current noise is to be non-trivial task and experimental results should be analysed with a great care. We suggest that most of peculiarities in GR noise measured in FETs are stipulated by the noise of leakage current. The results presented in this part show that the leakage current as well as its noise has the features that allows studying microstructure of the barrier layer and processes responsible for leakage current formation.

3.2.1. Experimental layout

The structures under study were grown on c-plane sapphire wafers by organic metallic vapour phase epitaxy. They consisted of an AlN nucleation layer followed by a 4 micrometer thick undoped GaN buffer layer, a 5 nm $Al_{0.15}Ga_{0.85}N$ spacer, a 10 nm Si-doped $Al_{0.15}Ga_{0.85}N$ carrier supply layer, and a 12 nm undoped $Al_{0.15}Ga_{0.85}N$ cap layer. Conventional technology was used for fabrication of source and drain contacts: Ti/Al/Ni/Au metallization with annealing at 900°C, while a Ni/Au layer was used for gate (Schottky) contact. The devices have the gate length of 0.7 micrometer, gate width of 100 micrometer, and drain-source spacing of 5 micrometer. A room temperature Hall mobility and 2DEG sheet electron density were measured as 1270 cm^2/Vs and $6x10^{12}$ cm^{-2}, respectively.

Current-voltage and noise characteristics of the HEMT were measured in both standard (as in chapter 3.1) and non-standard set-ups. In the former case the source (or drain) is grounded, the gate bias is supplied by a voltage source with zero impedance, and the noise voltage is taken on ungrounded channel output. In the latter case both source and drain are grounded, the gate bias is supplied via a load resistance, and the noise voltage is taken on the gate output. These measurements were done to distinguish the contribution of channel current and leakage one. Room temperature noise spectra of the channel current were investigated in the linear regime at different drain and gate voltages.

3.2.2 Leakage noise measurement results

The noise spectra of leakage current are shown in Fig.3.10. The spectra were measured in the regime with grounded source and drain and the noise voltage taken on the gate output. The shape of the spectra resembles that of a Lorentzian expected for GR noise. The temporal dependence of leakage current behaves itself like random telegraph signal (RTS) noise. It is seen in Fig.3.11 that RTS noise shows a very complex switching behaviour with at least two different RTS series. The latter points out an existence of different paths for leakage current.

It should be noted that increasing of the gate voltage (over the whole paper we deal with reverse bias) gradually transforms higher frequency RTS series into lower frequency one. Effect of the leakage current noise is clearly seen in Fig.3.12 where drain voltage noise spectral density measured in standard set-up is shown. At drain voltages V_D >200 mV excess noise obeys to a *1/f* law. A small bump is observed with decreasing of drain voltage. In some cases up to three bumps were resolved.

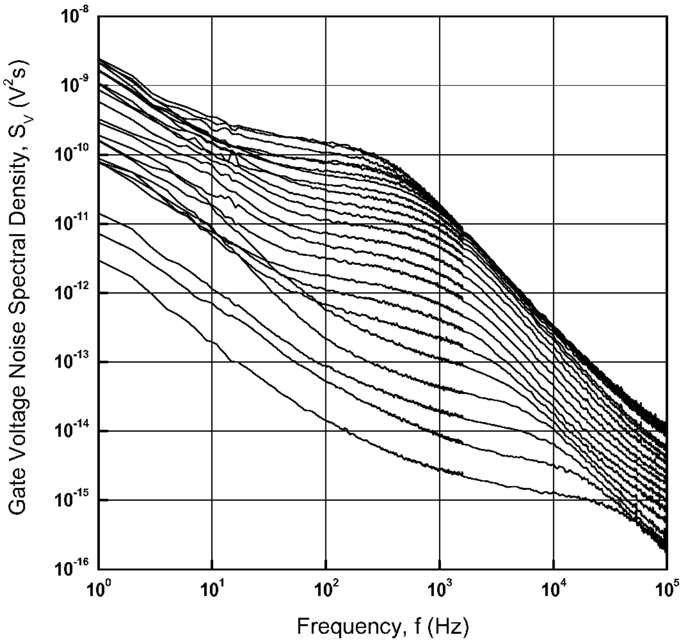

Figure 3.10 The noise spectra of leakage current measured at 300K in the regime with grounded source and drain and the noise voltage taken on the gate output. Gate voltage is changed from –0.7V (bottom) to –3.1V (top) with step 0.1V.

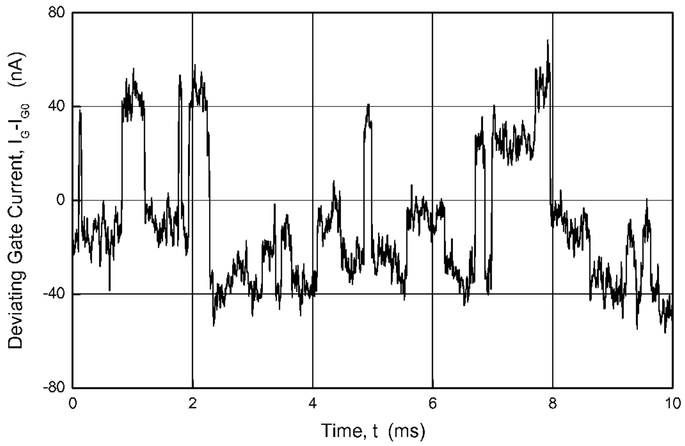

Figure 3.11 The temporal dependence of leakage current measured at 300K and gate voltage V_G=-3.1V.

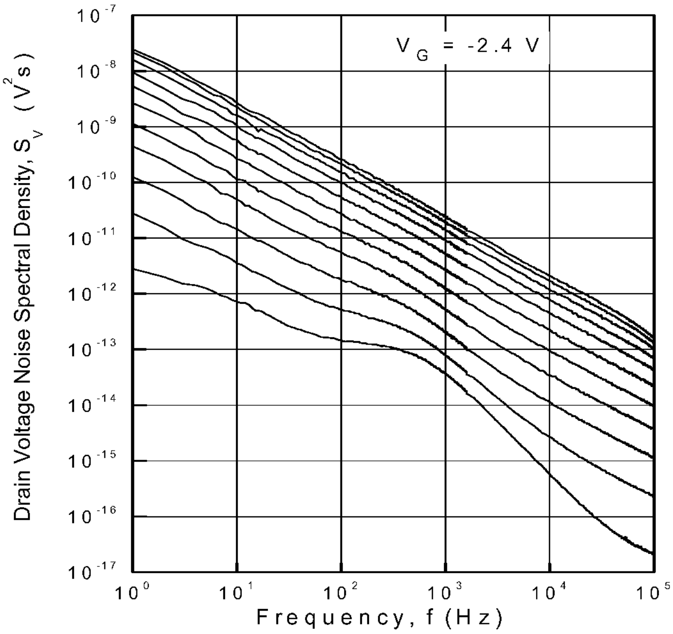

Figure 3.12. The drain voltage noise spectral density measured at 300K in standard setup at different source-drain voltages from 0V (bottom) to 500mV (top) with step 50mV.

Experimental data obtained clearly show that leakage currents cause all deviations of the noise spectra from *1/f* law. These currents exceed by several orders those predicted by a conventional tunnelling model. The origin of leakage current in different structures and devices should be quite different and depends on many factors concerned with technology as well as design. Most of researchers have suggested that defects might play a dominant role in the leakage current formation [58],[59]. In Ref.[60] the direct evidence has been presented that screw and mixed dislocations are primarily responsible for the reverse bias leakage in nitride materials. Analysis of current-voltage characteristics of our devices under study confirms an inhomogeneous spatial distribution of the leakage current. The leakage current reveals nearly linear dependence on the gate voltage that is an evidence of barrier-less carrier flow.

Our results of transport and noise properties could be explained if we assume that measured current consists of numbers of high-density randomly distributed current filaments formed by charges transferring along dislocation lines. The current is accompanied by fluctuations as a result of occasional changes of potential barrier height in the proximity of dislocation. The barrier modulation is caused by accidental capture/release of mobile carriers on/from defect centres neighbouring to dislocation area. Under these conditions amplitude of the current flowing throughout the dislocation is modulated synchronously to changes of defect's charging state. We suppose that fluctuating centres do not take direct participation in conductivity otherwise we should observe normal *1/f* or suppressed shot noise, though the latter requires additional proofs. Thus, we can consider observed RTS noise as fluctuations of charge accumulated on defect centres randomly distributed in the barrier layer, while the local high conductive channels as probes for their investigation.

In summary, a study of noise spectra and leakage current behaviour for different applied voltages allows to conclude that appearance of the bump is a result of GR noise attributed to the current flowing through the AlGaN barrier region. Current fluctuations arise as a result of accidental capture/release of mobile carriers on/from defect centres neighbouring to dislocation area. Parameters of the GR process were estimated from the analysis of the GR noise spectrum. The temporal dependence of leakage current behaves itself like RTS, which provides additional information about processes in the barrier. Two different RTS series in the current were observed. Studying of the leakage noise temperature dependence would be interesting continuation of the present work that can provide us with activation energies of these GR processes.

Chapter 4: Transport and noise properties of AlGaN HEMTs under gamma irradiation

In this chapter a structural, transport and noise properties of HEMTs irradiated by gamma-quanta are studied. Due to a strong chemical bonding the transistors are expected to be promising for broad applications in radiation environment [61]. Investigation of noise properties gives important information about defect structure in multilayer semiconductor heterostructures, especially if additional traps are introduced under external irradiation. Up to now, noise properties in irradiated HEMTs have not been investigated. At the same time, such investigations are very important not only from fundamental point of view for obtaining substantial information on the physical properties of semiconductor materials and devices but also it gives limiting values of the device performance for application in space environment. The measurements done in this chapter provide important information about radiation hardness of the HEMTs and their high potential in satellite system applications.

4.1 Investigation of radiation hardness of AlGaN HEMTs

AlGaN/GaN heterostructures, in spite of a lattice mismatch between epilayers of different alloy composition as well as the substrate, which may be a reason for structural defect formation, demonstrate unique noise properties [62]. Besides, due to a strong chemical bonding they are expected to be promising for broad applications in radiation environment [61]. Investigation of noise properties gives important information about defect structure in multiplayer semiconductor heterostructures, especially if additional traps are introduced under external irradiation. Up to now, noise properties in irradiated HEMTs have not been investigated. At the same time, such investigations are very important not only from fundamental point of view for obtaining substantial information on the physical properties of semiconductor materials and devices but also it gives limiting values of the device performance for application in space environment. It is essential that we introduce basic point defects by gamma irradiation in a controlling way. The changes in defect structure under gamma irradiation are usually accompanied by a charge carrier removal. Additionally, radiation induced transfer of the elemental components stimulated by ionisation processes takes place. In this chapter, the effect of gamma irradiation on I-V characteristics and low-frequency noise spectra of AlGaN/GaN HEMTs with nanoscale gate length are reported. These measurements provide information about radiation hardness of the HEMTs and their high potential in satellite system applications.

4.1.1 Experimental details

Transport and noise properties in AlGaN/GaN grown by metallorganic vapour phase epitaxy (MOVPE) on sapphire substrates have been studied before and after gamma irradiation. The device layer structure was the same as for samples investigated in chapter 2.1 of this work.

The transistor DC characteristic measurements were analysed with a HP4145B Semiconductor Parameter Analyzer.

The noise spectra were measured in the frequency range from 1 Hz to 100 kHz at room temperature using a low-noise preamplifier. The directly measured noise power spectral density was analysed by an HP35670A Dynamic Signal Analyzer. The devices were irradiated at room temperature by a ^{60}Co gamma rays source with doses in the range of 10^4-10^9 Rad and radiation flux of 10^2 Rad/s. The gamma-quantum average energy is about 1.2 MeV. The device temperature during irradiation did not exceed 40 ^{0}C. Measurements were performed within several hours after the irradiation procedure and several months later.

4.1.2 Transport properties of transistors after irradiation

Current-voltage characteristics measurement was used to examine the properties of HEMTs before and after gamma irradiation with a small step in radiation dose in order to reveal a critical dose at which operating parameters of the HEMTs show small changes. The radiation measurement cycle was repeated until visible changes were observed in the I-V characteristics. Surprisingly, for small radiation dose up to $7x10^5$ Rad, the basic parameters of the HEMTs, such as the saturation current I_S and transconductance, have been improved after irradiation (in Fig. 4.1 are shown results for I_S). The observed improvement can be explained by relaxation of existing strain and structural ordering of native defects. However, starting from the total dose of 10^6 Rad, we have observed only deterioration of the HEMTs operation parameters, which does not exceed 20 % for the highest radiation dose $1x10^9$ Rad investigated.

The comparison of the I-V curves of the HEMT devices with different gate lengths before and after the irradiation demonstrates the same behaviour. Namely, at small gate voltages the saturation current decreases with increasing gate voltage. At higher gate voltages, starting from some critical dose an opposite dose dependence was observed. The smaller the gate length the larger changes have been registered in the I-V characteristics. The transconductance decreases and threshold voltage V_T becomes more negative for all devices. The observable shift is about 0.7-0.9 V, and it can be entirely prescribed to changes in the sheet density $2x10^{12}$ cm^{-2} of the total charge ($\Delta\sigma$) in the barrier of the width d: $\Delta V_T = \Delta\sigma d/\varepsilon$ after the dose of $2x10^8$ Rad, where ε is the dielectric constant of the barrier material.

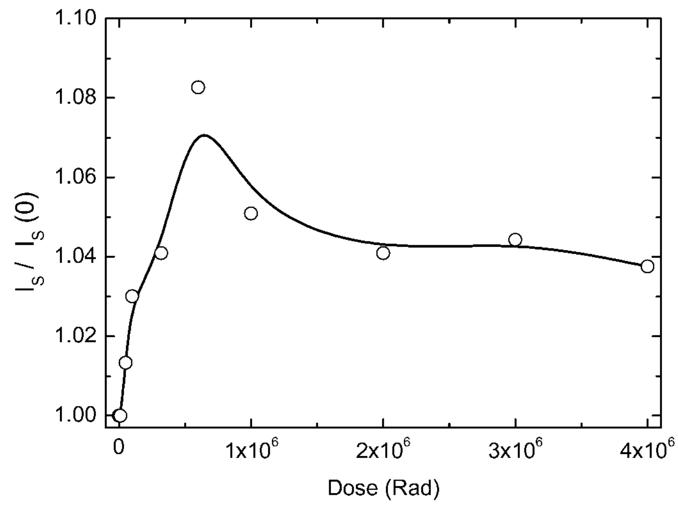

Figure 4.1. Normalized saturation current I_S / I_S (0) dependence on small radiation dose measured for HEMT device with 0.25 μm gate length and 200 μm gate width at V_{GS} =0.

Another experimental observation is considerable increase of leakage currents observed in heavily (1×10^9) irradiated devices. Besides, our study shows that in irradiated devices irreversible enhancement of the leakage current up to breakdown happens much more often than in pre-irradiated ones.

4.1.3 *1/f* noise measurement results after irradiation

Our HEMTs are three terminal devices and due to increasing of the leakage current after gamma irradiation one should carefully separate noise sources associated with channel current and additional leakage current noise, screening at some voltages the channel noise. We have measured the channel noise at different gate voltages in the regime where source-drain voltage was set equal to zero. After that the noise was measured with increasing V_{DS} in linear regime of the I-V characteristics to observe the noise level exceeding that due to the leakage current.

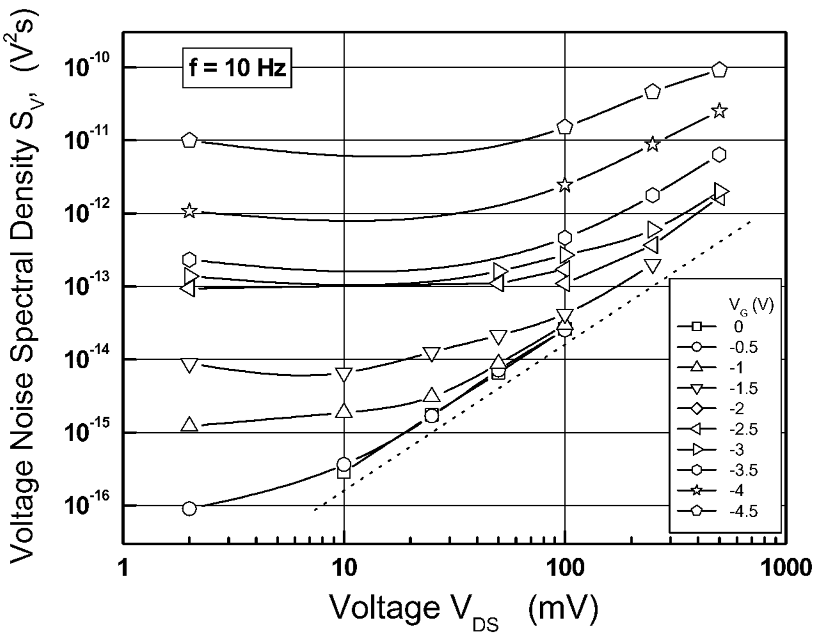

Figure 4.2 Voltage noise spectral density vs V_{DS} measured after 2.10^8 Rad dose. Dotted line shows $S_V \sim V_{DS}^2$. Leakage current noise measured at V_{DS}=0V is presented by symbols at V_{DS}=2mV

The experimental data show that at the high gate voltage and small voltage V_{DS} the excess noise is determined by the leakage current, and only for V_{DS} above 250 mV the intrinsic channel noise becomes dominant. It is interesting to note that in post-irradiated devices the leakage current noise increases with gate bias more rapidly than in the case of pre-irradiated HEMTs. The behaviour can be explained by deterioration of crystalline perfections of AlGaN layer under irradiation and additional spatial fluctuations of surface potential [63].

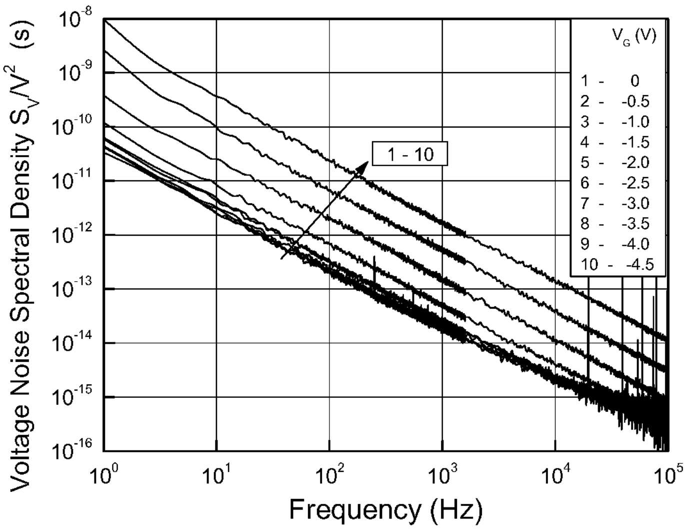

Figure 4.3 Normalized voltage noise spectra to voltage V_{DS} measured at different gate voltages after 2.10^8 Rad gamma-ray irradiation

Further, we will analyse the noise spectra measured at voltages V_{DS} corresponding to the channel noise level at least one order of magnitude larger than the leakage current noise. Typical experimental data for the HEMTs biased at fixed voltages measured at room temperature are shown in Fig. 4.3. The noise spectra after gamma-irradiation follow frequency dependence of the type of $1/f^{\gamma}$, with the exponent γ being close to one (*1/f* noise). At small gate voltages no deviation in noise level has been observed. The letter allows us to determine the Hooge parameter for passive and active regions separately, as it was done in the Chapter 3.1. The estimated value is about (0.4-1.8)x10^{-3} for the passive region and about (4-6)x10^{-4} for the active region. The Hooge parameter does not show a dependence on gate voltage and demonstrates high radiation hardness of the HEMTs to gamma irradiation that is in good agreement with mobility noise fluctuation model.

The transport and noise properties of AlGaN/GaN based HEMTs with gate length from 150 nm to 350 nm have been studied before and after gamma irradiation. The observed changes in the measured HEMTs characteristics can be interpreted in terms of additional defects produced by gamma radiation dose. The noise spectra demonstrate increasing role of leakage current after gamma irradiation, therefore, more detailed investigation of the influence of radiation on a leakage current is needed. The Hooge parameters determined separately for passive and active regions of the device show values three-five times larger after radiation dose $2x10^8$ Rad (~$1x10^{-3}$ for the passive region and about $5x10^{-4}$ for the active region). In general, results confirm, that due to their high radiation hardness, GaN-based HEMTs have good prospects on stability and reliability of devices intended for application in radiation environment.

4.2 Influence of gamma irradiation on leakage currents in GaN-based HEMTs

Investigations of gamma irradiated devices, made in chapter 4.1 of the present work, shows that most changes in transport and noise properties of the AlGaN/GaN HEMTs originate from changes in a leakage current. Therefore, more detailed investigations of this particular topic are needed to understand the mechanisms of the effect.

4.2.1 Experimental details

The same structures as in the previous chapter were used for investigation. The transistor DC characteristics were investigated with a HP4145B Semiconductor Parameter Analyzer operated in the transistor mode. The noise spectra were measured in the frequency range from 1 Hz to 100 kHz by a HP35670A Dynamic Signal Analyzer using a low-noise preamplifier ITHACO1201. All measurements have been carried out at room temperature.

Structural characterisation of the heterostructures has been performed by x-ray diffraction (XRD) and secondary ion mass spectroscopy (SIMS).

The gamma irradiation was provided by ^{60}Co gamma rays at room temperature with doses in the range of 10^4-10^9 Rad and flux of 10^2 Rad/s. The gamma quanta average energy was about 1.2 MeV.

4.2.2 DC measurements results

In the previous (3.1) chapter we have shown that due to enhanced radiation hardness of GaN-based HEMTs they have good prospects for applications in radiation environment. Moreover, an improvement of the principal parameters of the HEMTs, such as the saturation current and transconductance, was registered at the doses around $1x10^6$ Rad. It has been assumed the effect is related to relaxation of strains existing in mismatched heterostructures and structural ordering of native defects. To verify this suggestion we performed comparative study of structural and electrical characteristics of AlGaN/GaN HEMTs under small dose irradiation. Simultaneously, as-grown heterostructures used in further for the device fabrication have been examined after the same radiation treatment.

Except above-mentioned improvement of the dc parameters of the HEMTs after a low dose irradiation, there were negligible changes in the transfer characteristics. The peak position of the transconductance curve and the threshold voltage show a weak shift (~5%) towards lower (in absolute values; over the whole paper we deal with the gate biased negatively) gate voltages. An even more remarkable finding is a considerable decrease of dispersion of the transfer characteristics measured on a set of the transistors patterned on the same wafer (Fig.4.4). This is consistent with the higher uniformity of the irradiated heterostructure relative to non-radiated one.

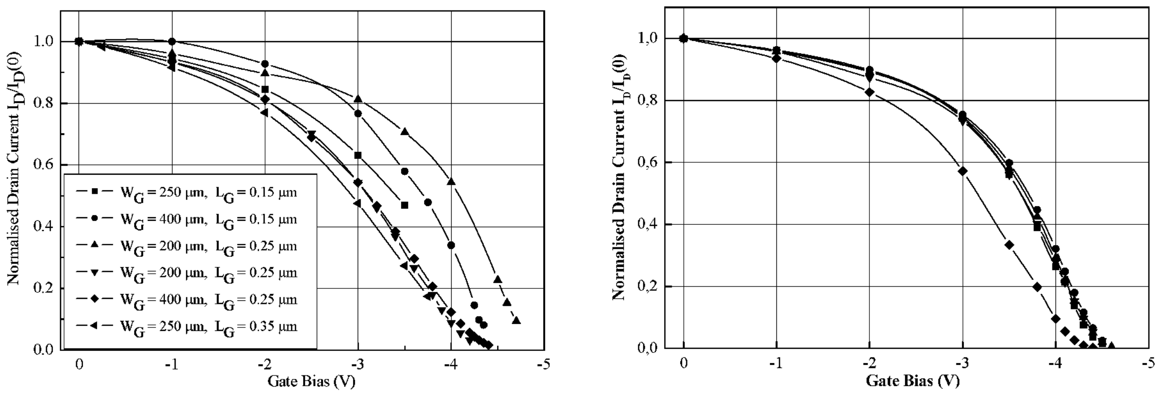

Figure 4.4. Normalised transfer characteristics for set of pre-radiated (left) and irradiated (right) at 1x10^{6} *Rad HEMTs,* U_{SD} *= 100 mV, T =300K.*

4.2.2 X-Ray diffraction measurements

To gain insight into structural transformation of the heterostructure during irradiation, x-ray diffraction of the wafers was performed at room temperature. Figure 4.5 shows the x-ray diffraction spectra of the AlGaN/GaN/Al_2O_3 wafer before and after 1x10^{6} Rad dose.

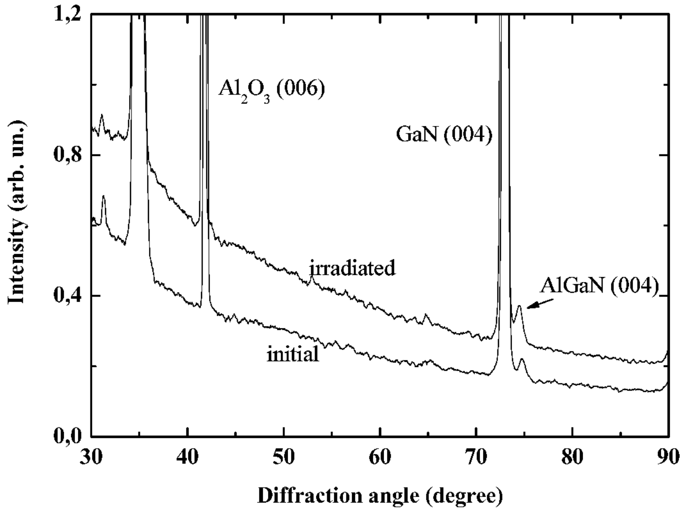

Figure 4.5. X-ray diffraction spectra for AlGaN/GaN heterostructure before and after $1x10^6$ Rad irradiation

It is worth to note the changes occurring with the reflection around the 74^0 (the reflection corresponds to the (004) plane of the AlGaN layer). Although the intensity of the peak is low, it is clearly seen its increasing and shift to lower 2θ position after irradiation. The later should be considered as a result of strain relaxation in the AlGaN layer. To prove this statement direct measurement of elastic strains existed in the heterostructure has been carried out. An integrated method for measuring of surface curvature, R was used to estimate the elastic strains [64]. The method consists in measurement of angle shift, α, of the diffraction maxima at translation of the sample on certain distance, *l*. The results of these measurements are presented in Fig.4.6. Negative sign corresponds to tensile stress in the AlGaN layer. It is clearly seen that strain relaxation does occur up to doses of $1x10^6$ Rad.

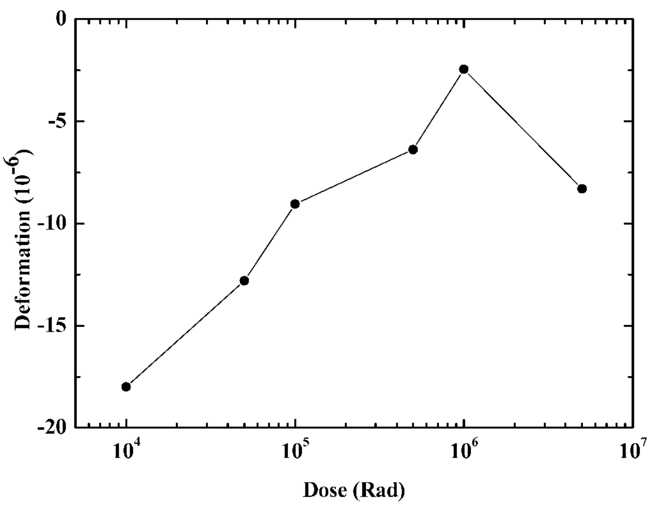

Figure 4.6. Dose dependence of elastic strains of the AlGaN layer.

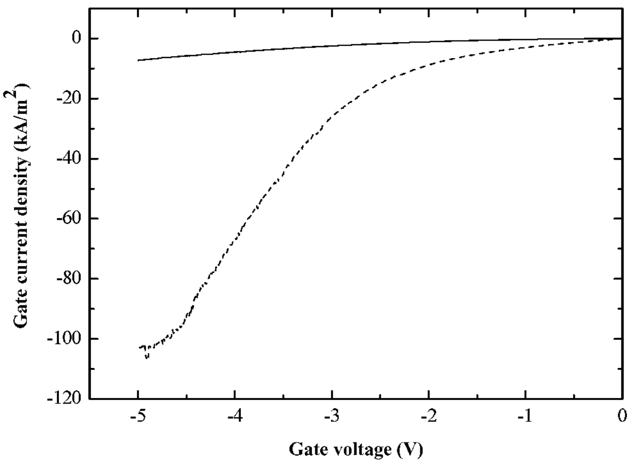

Figure 4.7. The gate-source current as function of gate voltage before (dashed curve) and after 1x10^{6} Rad irradiation (solid curve) measured at 300 K.

The results of structural measurements fairly agree with the electrical behaviour of the transistors. In particular, a considerable decrease of leakage current was established after low dose irradiation (Fig.4.7). The latter is accompanied by a decrease of leakage current noise.

4.2.3 Low-frequency noise measurements

Due to its important role in the device performance we paid special attention to the noise measurements. We know from our investigations in chapter 3.2, that peculiarities observed in the low frequency generation-recombination (GR) noise that is additional to *1/f* noise are connected with current flowing through the AlGaN barrier region. Therefore, studying of the features will allow us to investigate microstructure of the barrier layer and processes responsible for leakage current formation. It is necessary to point out that the Si_3N_4 passivation of the surface of the devices has been implemented to eliminate the surface leakage [65]. Noise characteristics of the HEMTs were measured in both standard and non-standard set-ups. In the former case the source (or drain) was grounded, the gate bias was supplied by a voltage source with zero impedance, and the noise voltage was taken on ungrounded channel output. In the latter case both source and drain were grounded, the gate bias was supplied via a load resistance, and the noise voltage was taken on the gate output. These measurements were done to separate the contribution of channel and leakage current contribution. Room temperature noise spectra of the channel current were investigated in the linear regime at different drain and gate voltages.

The noise spectra of the leakage current measured for pre-radiated device are shown in Fig. 4.8. The spectra were measured in the regime with grounded source and drain and the noise voltage taken on the gate output. The shape of the spectra resembles that of a Lorentzian expected for GR noise. The temporal dependence of leakage current behaves itself like random telegraph signal (RTS) noise. It is seen in Fig. 3.11 that RTS noise shows a very complex switching behaviour. It should be noted that increasing of the gate voltage gradually transforms the frequency of the RTS series. An analysis of the leakage current noise spectra shows that the observed RTS noise is caused by fluctuations of charge accumulated on defect centers randomly distributed in the barrier layer.

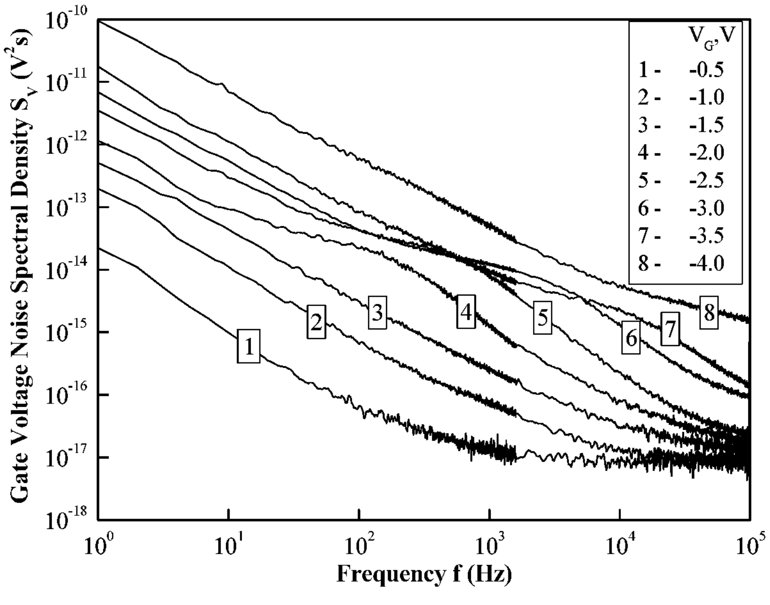

Figure 4.8. The noise spectra of leakage current for pre-radiated HEMT measured at 300 K in the regime with grounded source and drain and the noise voltage taken on the gate output. The gate width and length are 250 μm and 0.15 μm respectively.

The measurements performed on irradiated devices reveals a reduced level of the leakage current noise. Its temporal dependence is characterized as more stable and in most cases the RTS noise did not appear. All these findings are consistent also with the proposed mechanism of structural-impurity ordering that occurs in the barrier layer at initial irradiation stages.

It should be noted that the level of the channel current noise slightly increases even at small irradiation doses but these changes do not affect seriously on the reliable performance of the AlGaN/GaN HEMTs. The study of radiation effects on the channel current noise is another very interesting topic, not covered, however, by this work as it requires number of additional investigations.

In this chapter the investigation of small dose effects on operational parameters of AlGaN/GaN HEMTs was carried out. It was shown that transport and noise characteristics of the transistors reveal a tendency to improvement under irradiation by gamma-quanta up to doses of 10^6 Rad. The effect is explained by relaxation of elastic strains and structural ordering of native defects in the AlGaN barrier layer. The suggestion is confirmed by results of structural characterization of as-grown heterostructures after the same radiation treatment.

Chapter 5: Phase Noise Study of an AlGaN/GaN HEMT X-Band Oscillator

Low phase noise oscillators are the key component of modern microwave communication system with reduced rate of bit errors and high sensitivity doppler radar systems. AlGaN/GaN HEMT-based monolithic microwave integrated circuit (MMIC) oscillators have attracted increasing interest as devices especially promising for microwave power application due to fundamental properties of a gallium nitride heterostructures, such as wide band gap and high electron drift velocity [31,44]. Strong polarization fields allow accumulating high electron density of two-dimensional electron gas (2DEG) at the heterointer-faces of AlGaN/GaN structure without intentionally doping in the barrier [30]. In the case of an undoped heterostructures the electrons of 2DEG are characterized by high mobility due to absence of scattering doping centres. Additionally the decrease of the level of a phase noise in the amplifier or oscillator is expected. The nitride structures well suited for 16.5 W/mm of gate periphery output power levels [66] with 47% power added efficiency. This material system can be useful for the oscillator circuit design where phase noise level strongly depends on output power and can be reduced inversely proportional to the power. In this chapter *1/f* baseband noise of AlGaN/GaN HEMT and its up conversion coefficient to the oscillator phase noise for the case of MMIC AlGaN/GaN oscillator are studied and analysed.

5.1 Fabrication and design

To optimize parameters of the oscillator we have used results of investigation of thermal and noise properties of AlGaN/GaN transistors, carried out in chapters 2, and 3 of the present work. The layers of oscillator were grown on semi-insulating SiC substrate instead of sapphire for its increased conductivity. Barrier thickness and height was slightly increased to reduce a noisiness of the device.

Epitaxial layers were grown by metalorganic vapour phase epitaxy. First, an AlGaN nucleation layer is grown on the (0001) surface of a SiC substrate followed by an AlN(200nm) layer. Then, 1μm thick GaN buffer layer is deposited. Finally, approximately 25nm thick layer of undoped $Al_{0.35}Ga_{0.65}N$ is grown. Hall measurements show existence of two-dimensional electron gas (2DEG) at the interface with sheet charge concentration of $1.2x10^{13}cm^{-2}$ and room mobility around 1200 $cm^2/(Vs)$. Typical DC parameters of the device after fabricating the ohmic and gate contacts are: open-channel circuit density=100 mA/mm, peak transconductance=200 mS/mm, pinch-off voltage = - 6V.

Device fabrication on grown epitaxial layers starts with the deposition of Ti/Pt alignment marks for e-beam- and photolithographies. Mesa isolation is then photolithographically patterned and etched with chlorine-based ECR plasma.

Ti(20nm)/Al(100nm)/Ti(45 nm)/Au(55 nm) ohmic contacts are patterned with e-beam lithography, deposited with e-gun evaporation and annealed at 800^0C for 60 seconds. Ohmic contact resistance and sheet resistance, measured using TLM method, were equal to 0.5 Ohm-mm and 500 Ohm/square respectively. Ni(25nm)/Au(375nm) mushroom gates are written with an e-beam, developed using triple resist stack of PMMA/Copolymer/PMMA and deposited with e-gun evaporation. The mushroom gate structure is designed with dimensions that prevent the passivation (the step to follow) from reaching the metal edge of the gate footprint on the drain side. This is done to preserve the breakdown voltage and gate leakage of the unpassivated transistor. The first interconnect level is defined by photolithography and uses deposition of 3500 Å of Au to form the contact pads. Preliminary device characterization is then performed. Following that, an 1800 Å thick CVD Si_3N_4 film is deposited in order to passivated the surface. The second interconnect level processing, which consists of via hole etching, airbridge post definitions and deposition, seed layer evaporation and electrochemical plating of 3μm thick Au, concludes the device fabrication sequence.

The common gate oscillator architecture was used as a basis for the design because it maximizes device instability in comparison with the common-source architecture. It is also considered the more appropriate option for high power oscillators.

Following typical procedure for design of a two-port negative resistance oscillator, measured common-source small signal S-parameters of a 10-channel HEMT with 1.5 mm total gate periphery and measured f_t=27 GHz and f_{max}=36 GHz were converted to common-gate S-parameters. An output matching network, placed across the HEMT's drain-gate junction, was designed to maximize the input reflection coefficient at 10 GHz. The resonator circuit, placed across the HEMT's source-gate junction is designed as :

$$Z_{resonator} = -\frac{R_{in}}{3} - jX_{in}, \qquad (5.1)$$

where R_{in} and X_{in} are real and imaginary parts of the common-gate HEMT's input impedance.

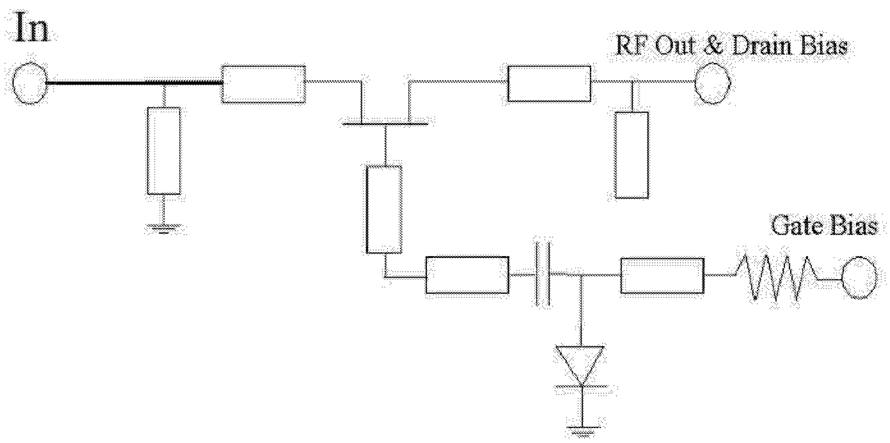

Figure 5.1 Schematic configuration of the AlGaN/GaN MIMC voltage controlled oscillator (VCO).

Output and resonator networks with varactor diode as a part of the resonator are implemented with coplanar waveguide transmission lines based on known small-signal models. Gate bias network uses MIM capacitors and a bulk resistor. Due to asymmetric connection of the resonator to the HEMT's source electrode, the measured value of source inductance (10 pH) is added in series with the source. The oscillator schematic is shown in Figure 5.1. The oscillator was characterized on-wafer with air-coplanar probes. Oscillator input was terminated with a short. SEM image of the monolithic oscillator is shown in Figure 5.2.

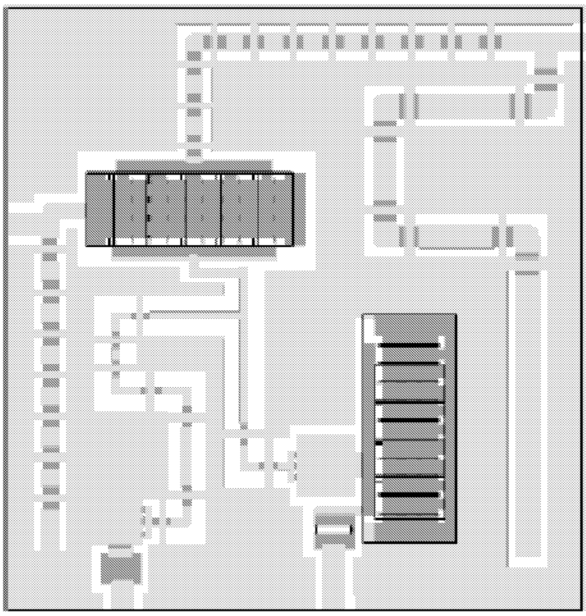

Figure 5.2. Layout of the AlGaN/GaN MIMC VCO. Size of the chip approx. 1.6×1.6 mm.

5.2 Measurement technique

The output power spectrum of the oscillator was measured with Agilent 8562A Spectrum Analyzer at different drain voltages. The oscillator delivers 28 dBm at 9.335 GHz when biased with V_{DS}=28V and V_{GS}= - 4.2V. A phase noise of monolithic X-band oscillator, based on AlGaN/GaN HEMT with 1.5mm total gate periphery, has been investigated. Phase noise of the oscillator was measured with HP E5500 Phase noise measurement system. Signal from the oscillator was connected to the input of HP 70422A downconverter. Downconverted to 335MHz signal was transferred to HP 70420 A Test set signal input, where beatnotes has been established between the downconverted oscillator signal and the reference signal from HP 8662 Signal generator. A necessary frequency difference was maintained by tuning of the oscillator signal with internal VCO of the downconverter. In opposite to traditional technique, where the reference signal is tuned, this method proved to be more reliable in the case of high power RF oscillators.

The phase noise of the system was analyzed in range of offset frequencies from 10 Hz to 100 MHz.

5.3 Low frequency noise results

The low frequency *1/f* noise is one of the important factors that limit the oscillator phase noise performance. Using the methods, developed in the chapters 2 and 3 of the present work, we studied the flicker noise characteristics of AlGaN/GaN high electron mobility transistors grown on SiC substrate by metal organic chemical vapour deposition. Low frequency noise spectra were measured at different gate source and drain-source voltages in the common source configuration. Fig. 5.3 shows the drain-source voltage noise at different drain biases at certain gate voltage. The dependence of the noise on gate bias is small, but the noise increases with larger drain-source bias voltages. Dimensionless Hooge parameters [22] were calculated for frequency 1 kHz by equation (3.1) as explained in the chapter 3. For the spectra presented in Fig. 5.3 its value was found to be about $\alpha_H = 4\text{x}10^{-4}$. This value of the Hooge parameter is comparable to the noise level of commercial GaAs heterostructures devices.

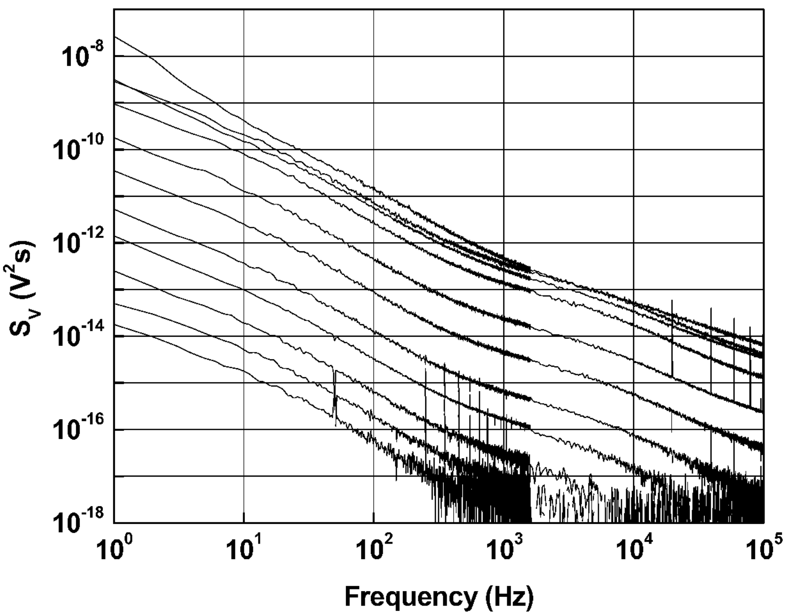

Figure 5.3. Low frequency noise spectra measured at Vgs = - 4V and different drain voltages Vds (V): 0.005, 0.010, 0.020, 0.050, 0.100, 0.250, 0.500, 1.000, 2.000, 4.000, 28.000 (shown on the figure from bottom to the top)

A deviation of low-frequency noise from *1/f* dependence has been observed upon increasing the applied voltage, while the high frequency normalized to resistance *1/f* component remains without changes during the increasing of applied voltage. Fig. 5.4 shows this behaviour of the low frequency noise for the biases in our oscillator, as it will be described later. The effect of increased noise level at small frequencies superimposed to the flicker *1/f* noise source correlates with non-linearity of current-voltage characteristics of the HEMT and can be explained by increased dissipated power in the device.

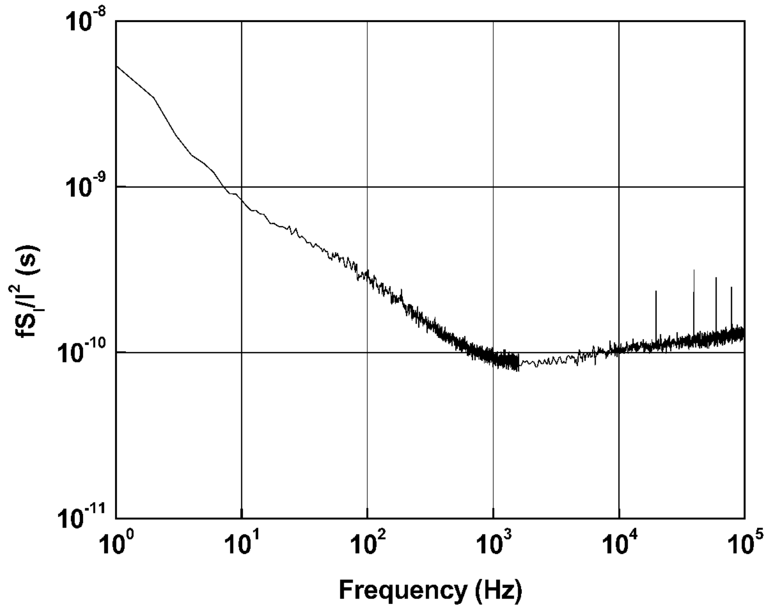

Fig. 5.4. Normalized low frequency noise spectra measured at Vgs = - 4V and Vds = 28V.

5.4 Up-conversion of low frequency noise to the phase noise of the oscillator

In a feedback-oscillator the output signal of a low *1/f* – noise microwave amplifier is passed through a two-port microwave resonator and fed back to the amplifier input. If the total phase in oscillator equals to 2π and the total loop amplification exceeds unity, the device oscillates at the resonant frequency of the resonator selected by filter. The phase noise in the resonator circuit is minimized under the optimal relation between the quality factors of loaded to unloaded resonator $Q_L = Q_U/2$ [67], which is usually established by the coupling port conditions.

The basic phase noise behaviour of the oscillator circuit is described by the Leeson model [68], which describes the main noise sources of the oscillator. According to this model the phase noise comprises both resonator (the first term) and amplifier (the second term) contribution given by Eq.(5.2):

$$L_{osc} = 10 \cdot \log\left[1 + \frac{f_0^2}{4Q_L^2 f_m^2}\right] + 10 \cdot \log\left[\frac{\alpha}{f_m} + \frac{GFkT}{P}\right] \tag{5.2}$$

The amplifier noise consisting of the white noise determined by the amplifier gain G, noise figure F, temperature T and output power P. In addition, there is $1/f$ noise leading to a fluctuation amplitude α/f_m at the offset frequency distanced by $\pm f_m$ from the carrier frequency f_0. According to equation (5.2) the phase noise of the oscillator exhibits a $1/f_m^3$ dependence in a certain range of offset frequencies. The noise decreases strongly upon increasing the loaded quality factor Q_L of the resonator. Up to now the highest Q_L is achieved in resonators designed on the base of dielectric sapphire or superconducting materials due to extremely low intrinsic losses.

The measurement and calculation results of phase noise spectrum for the GaN-based MMIC oscillator is shown at Figure 5.5 for two different loaded quality factors Q. The AlGaN/GaN oscillator exhibits –30 dB/decade up to 10 MHz and is dominated by the $1/f$ noise of the HEMT.

Very low level of the phase noise was observed. At 100 kHz offset the phase noise equals to –105 dBc/Hz, which is among best reported results for an X-band MMIC oscillators. The value is close to the phase noise, calculated from the Leeson model [69], which is based on phase noise properties of the oscillator components. Our results demonstrate, that the phase noise performance of the AlGaN/GaN MMIC oscillators are better then the noise of the best GaAs- and GaN-based oscillators (Fig. 5.5). For conventional GaAs oscillators the up-conversion factor, which is important for phase modulation in modern telecommunication system, is about 40-90 MHz/V [70] for an offset frequency of 100 kHz when MMIC technology was used. The up-conversion factor in our oscillators calculated accordingly

Eq. (11) of Ref.[71] is about 15 MHz/V for the same offset frequency, which results in low oscillator phase noise of -105 dBc/Hz.

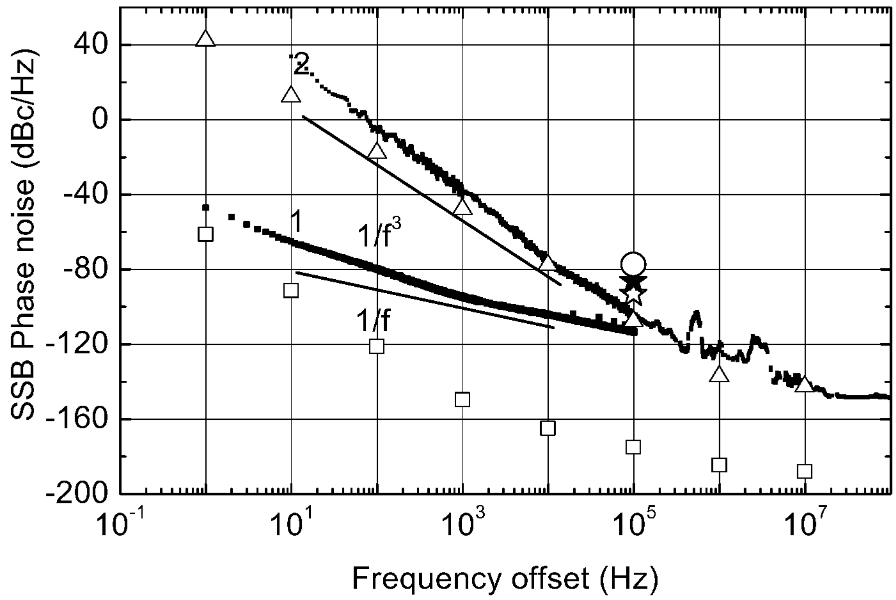

Figure 5.5 Phase noise measurement results at U_{GS} = - 4 V and U_{DS} = 28 V (curve 1 – for HEMT structure plotted as dBc, curve 2 - for oscillator based on the HEMT) and simulated results accordingly to Leeson model (open triangular – for Q=20, open square – for Q=3000000) compared to the noise value (normalized to the same frequency) : open star – GaAs HBT oscillator, closed star – GaN FET, open circle – GaAs FET (See Ref.[72]).

In spite of low quality factor of the resonator about 20 the AlGaN/GaN HEMTs makes a good choice for use in microwave local oscillator applications. If assembled with high quality whispering-gallery dielectric resonator (with Q ≈ $3x10^6$) the phase noise value can be decreased down to –175dBc/Hz at 100 kHz.

In conclusion, a low phase noise GaN MMIC oscillator has been presented, in conjunction with the study of the low frequency noise. The oscillator has demonstrated remarkably good performances with low phase noise and the high output power. The oscillator delivers an output power of 28 dBm with DC-to-RF efficiency of 16%. The measured phase noise is –105 dBc/Hz at 100 kHz offset from 9.35 GHz carrier with only 15 MHz/V up conversion factor, which is better then of MMIC oscillators built on GaAs HEMTs.

Chapter 6: Conclusion and Outlook

Semiconductor electronics plays a very important role in the modern world. Demands for operation speed and power are increasing every year significantly and usual materials cannot longer keep the pace. The unique properties of GaN-based heterostructures allow raising standards of efficiency, power handling and sensitivity.

In this work, the fundamental properties of GaN/AlGaN HEMT structures have been investigated in order to optimize their performance in high power microwave devices. Systematic studies of electronic, noise and structural properties have been performed.

We have started from the investigation of Joule heating effects and DC transport properties in polarization induced 2DEG channels. The gateless TLM structures have been suggested for adequate analysis of the transport effects. The observed current saturation through a TLM structure confirms that both thermal overheating and hot electron effects are influencing the current. A theoretical model has been developed for the separate investigation of both relevant effects. We performed microsecond pulse measurements that show a 60% reduction of self-heating influence compared to DC measurements, which is in agreement with our calculations. According to our results, nanosecond pulses are required to remove thermal overheating effects, which have a big influence on HEMT characteristics under normal operation voltages. To utilize the unique properties of group III-nitride heterostructures, including the high speed of the electrons, it is therefore necessary to optimize the thermal budget of the devices.

In order to remove Joule heating effects and to investigate only the fundamental transport properties, we developed a nanosecond pulse measurement technique. By applying 10-30 ns electrical pulses to AlGaN/GaN gateless heterostructures, we experimentally measured low field and high field transport phenomena, including the drift velocity dependence on the applied electric field up to the record height of 150 kV/cm for GaN-based heterostructures. Particularly, a current density above 1.5 A/mm was measured at high voltages. It is remarkable, that despite the measured nitride structures had moderate values of low-field electron mobility, we obtained a drift velocity of 1.7×10^7 *cm/s* at a field of 150 *kV /cm*. This value is still lower than the theoretical limit (~3×10^7 *cm/s*). However it is very close to the values V_{dr} measured for perfect modulation doped AlGaAs/GaAs structures.

Besides the self-heating, another strong limitation of high frequency devices is low-frequency noise. We investigated *1/f* noise properties of the 2DEG as well as leakage noise in HEMT transistors. The separate investigation of noise related to active (gated) and passive (ungated) regions of HEMTs was, for the first time, done in AlGaN/GaN devices. The temperature dependence of the noise revealed a characteristic transition frequency from the *1/f* dependence to a stronger one. The process has an activation energy of 0.4 eV, which can be related to traps in the AlGaN barrier.

The leakage noise, instead, manifested itself as a generation-recombination (GR) noise. It was found that current fluctuations arise as a result of accidental capture/release of mobile carriers on/from defect centres in the vicinity of dislocation areas. Parameters of the GR process were estimated from the analysis of the GR noise spectrum. The temporal dependence of the leakage current behaves like random telegraph signal (RTS), which provides additional information about the GR process, and, consequently, about the defect structure of the barrier.

The investigation methods that were developed proved to be very useful for studying the influence of gamma irradiation on our structures. The transport and noise properties of AlGaN/GaN based HEMTs with gate length from 150 nm to 350 nm have been studied before and after gamma irradiation up to $1\text{x}10^9$ Rad doses. The observed changes in the measured HEMT characteristics were interpreted in terms of additional defects produced by gamma radiation. The noise spectra demonstrate the increasing role of leakage current after high gamma irradiation dose. The Hooge parameters, determined separately for passive and active regions of the device, show values three to five times larger after a radiation dose of $2\text{x}10^8$ Rad (~$1\text{x}10^{-3}$ for the passive region and about $5\text{x}10^{-4}$ for the active region). Still, even after the highest dose, devices can operate on an acceptable level. In general, the results confirm, that due to their high radiation hardness, GaN-based HEMTs have good prospects for stability and reliability of devices intended for application in radiation environment, particularly for space applications.

Even more promising appeared to be the small dose results. It was shown that transport and noise characteristics of the transistors reveal a tendency to improvement under irradiation by gamma-quanta up to doses of 10^6 Rad. The effect was explained by relaxation of elastic strains and structural ordering of native defects in the AlGaN barrier layer. The suggestion was confirmed by results of structural characterization (X-ray diffraction measurement) of as-grown heterostructures after the same radiation treatment.

In the final part of this work, we have used our experience, gained during the investigation of transport and noise properties of our transistors, to optimize the parameters of the integrated circuit oscillator. To optimize the thermal budget, HEMT layers were grown on semi-insulating SiC substrate instead of sapphire. Slight improvement of the barrier thickness and height as well as particular attention to the quality of gate contacts allowed us to achieve a lower level of *1/f* noise. As a result, a low phase noise GaN MMIC oscillator has been presented, in conjunction with the study of the low frequency noise. The oscillator has demonstrated remarkably good performance with low phase noise and high output power. The oscillator delivers an output power of 28 dBm with DC-to-RF efficiency of 16%. The measured phase noise was -105 dBc/Hz at a 100 kHz offset from 9.35 GHz carrier with only 15 MHz/V up conversion factor, which is better then the noise measured for MMIC oscillators built on GaAs HEMTs.

These investigations revealed further ways to optimize GaN-based HEMTs than was described here. Particularly, the influence of surface passivation at low frequency noise need to be studied in detail. Our recent experimental results have shown, that increasing Al concentration up to 75% in the heterostructure barrier can drastically reduce the noisiness of the channel. Optimizing the ohmic contact technology is needed in this case, however, due to increase of the contact noise. Temperature investigations of leakage noise can give us additional information about defect states in the barrier and lead to new ideas of reducing the leakage currents.

These questions are still left open. They are promising even more fascinating results for GaN-based heterostructures in the field of high speed, high power and low noise applications.

Appendix

Solution of Laplace equation for heat dissipation

Distribution of heat in AlGaN/GaN-based heterostructures grown on sapphire is mostly determined by sapphire substrate itself. It usually two orders of magnitude thicker and has much lower thermal conductivity as compared to GaN. Therefore in our model we will consider distribution of heat from hot zone on top of sapphire substrate while assuming that bottom of the substrate is in adiabatic conditions.

Schematic of this model is shown in Fig.A.1. Hot zone is greyed out.

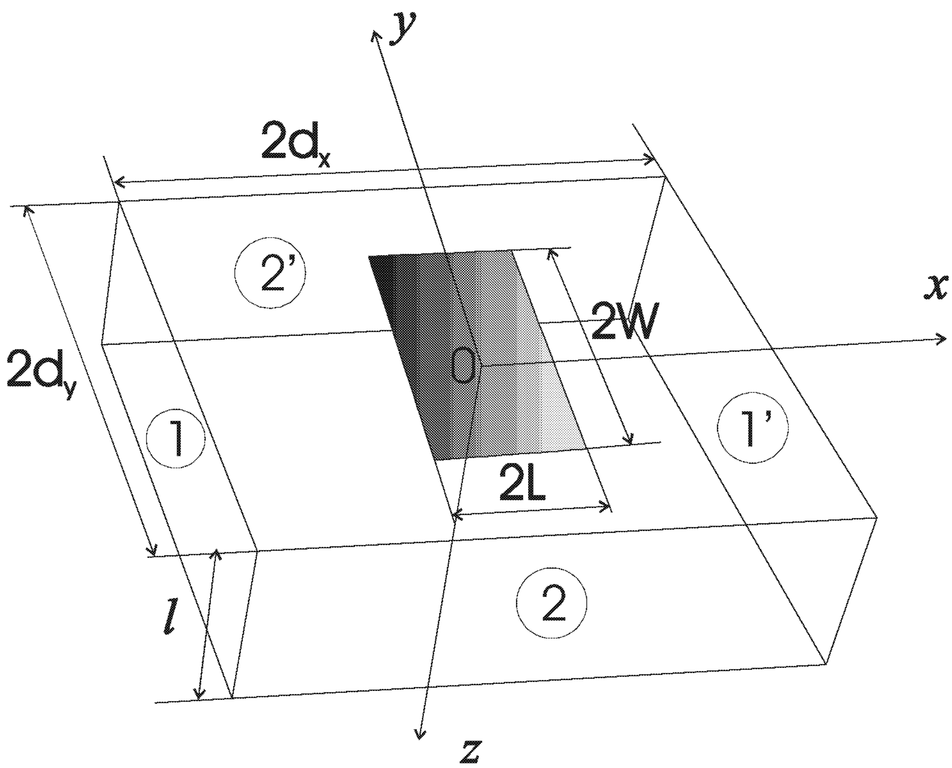

Figure A.1. Model of the heat dissipation

Let us write Laplace equation for heat distribution:

$$\frac{\partial^2 T}{\partial x^2}+\frac{\partial^2 T}{\partial y^2}+\frac{\partial^2 T}{\partial z^2}=0 \tag{A.1}$$

Assume a separable solution: $T(x,y,z)=X(x)Y(y)Z(z)$. In this case Eq. (A.1) will transform to:

$$YZ\frac{\partial^2 X}{\partial x^2}+XZ\frac{\partial^2 Y}{\partial y^2}+XY\frac{\partial^2 Z}{\partial z^2}=0 \tag{A.2}$$

$$\frac{X''}{X}+\frac{Y''}{Y}+\frac{Z''}{Z}=0 \tag{A.3}$$

Let $\frac{X''}{X}=-\alpha^2=-\left(\frac{Y''}{Y}+\frac{Z''}{Z}\right)$, where α is a separable constant. Then $\frac{Y''}{Y}=\alpha^2-\frac{Z''}{Z}=-\beta^2$.

This leads us to system of equations:

$$\begin{cases} X''+\alpha^2 X=0;\ X\sim e^{kx}, & k^2+\alpha^2=0,\ k=\pm\alpha i, \\ Y''+\beta^2 Y=0;\ \ Y\sim e^{ky}, & k^2+\beta^2=0,\ k=\pm\beta i, \\ Z''-\gamma^2 Z=0,\ \ \gamma^2=\alpha^2+\beta^2;\ k^2-\gamma^2=0, & k=\pm\gamma. \end{cases} \tag{A.4}$$

Accordingly, separable solutions are of the form:

$$T(x,y,z)\sim e^{\pm i\alpha x}\cdot e^{\pm i\beta y}\cdot e^{\pm\gamma z} \tag{A.5}$$

Now we shall write boundary conditions for our sample.

At side edges (surfaces 1, 1’, 2, 2’ of Fig. A.1):

1 and 1’:

$$\frac{\partial T}{\partial x}=0 \tag{A.6}$$

$x=d_x;\quad -d_y\le y\le d_y;\quad 0\le z\le l;\qquad$ (a)

$x=-d_x;\quad -d_y\le y\le d_y;\quad 0\le z\le l.\qquad$ (b)

2 and 2’:

$$\frac{\partial T}{\partial y}=0 \tag{A.7}$$

$y=d_y;\quad -d_x\le x\le d_x;\quad 0\le z\le l;\qquad$ (a)

$y=-d_y;\quad -d_x\le x\le d_x;\quad 0\le z\le l.\qquad$ (b)

At bottom edge of our sample:

$$T(x,y,z=l)=0 \tag{A.8}$$

$$-d_x \le x \le d_x; \quad -d_y \le y \le d_y; \quad z=l.$$

At top edge in the hot zone:

$$-\lambda\frac{\partial T}{\partial z}=q=\frac{P_{dis}}{4WL}. \qquad \frac{\partial T}{\partial z}=-\frac{q}{\lambda}. \tag{A.9}$$

$$z=0; \quad -L\le x\le L; \quad -W\le y\le W$$

At the top outside the hot zone:

$$\frac{\partial T}{\partial z}=0 \tag{A.10}$$

$$z=0;\ L\le x\le d_x; \qquad -d_y\le y\le d_y; \qquad \text{(a)}$$

$$-d_x\le x\le -L; \qquad -d_y\le y\le d_y; \qquad \text{(b)}$$

$$-L\le x\le L; \quad W\le y\le d_y; \qquad \text{(c)}$$

$$-L\le x\le L; \quad -d_y\le y\le -W \qquad \text{(d)}$$

Firstly, we shall use boundary conditions (A.6) and (A.7) on lateral edges 1,1' and 2,2' (Fig.A.1).

$$T(x,y,z)\sim\cos(\alpha x)\cdot\cos(\beta y)\cdot e^{\pm\gamma z}, \ X\sim\cos(\alpha x) \qquad X'\sim\sin(\alpha x) \tag{A.11}$$

For $\left.\frac{\partial T}{\partial x}\right|_{\pm d_x}=0$ this yields $\sin(\alpha x)=0$ or $\alpha_n x=n\pi$, $n=0,\pm1,\pm2,\ldots$, from which only $n=1,2,\ldots$ are different and essential for the solution.

Similarly, for conditions (A.7) we obtain $Y\sim\cos(\beta y)$, $Y'\sim\sin(\beta y)\Rightarrow\beta_m={}^{m\pi}/_{d_y}$, $m=1,2,\ldots$

Thus, we find: the only possible values for the separable constants are as follows:

The corresponding eigenfunctions are:

$$X \sim \cos(\alpha_n x), \alpha_n = {}^{n\pi}/_{d_x}, \; n = 1,2,... \tag{A.12}$$

$$Y \sim \cos(\beta_m y), \beta_m = {}^{m\pi}/_{d_y}, \; m = 1,2,... \tag{A.13}$$

Consequently, $\gamma_{nm}^2 = \pi^2 \left[\left(\frac{n}{d_x} \right)^2 + \left(\frac{m}{d_y} \right)^2 \right]$.

It should be noted that the case of zero α, β and γ should be considered separately.

Now we use boundary conditions on the bottom and top edges.

$$Z \sim ce^{\gamma z} + de^{-\gamma z} \tag{A.14}$$

At the bottom $(z = l)$:

$$Z_{(z=l)} = ce^{\gamma l} + de^{-\gamma l} = 0 \Rightarrow d = -ce^{-2\gamma l}$$

Putting this result in (A.14) we get:

$$Z = ce^{\gamma z}\left[1 - e^{2\gamma(l-z)}\right] \tag{A.15}$$

The separable solution then built using (A.12), (A.13) and (A.15):

$$T_1(x, y, z) = \sum_{n,m=1}^{\infty} C_{nm} \cdot \cos\left({}^{\pi n x}/_{d_x}\right) \cdot \cos\left({}^{\pi m y}/_{d_y}\right) \cdot e^{\gamma z}\left(1 - e^{2\gamma(l-z)}\right) \tag{A.16}$$

Now we can use boundary conditions (A.9) and (A.10) for the top edge of the structure. After differentiation of (A.16) on z we get:

$$\frac{\partial T_1}{\partial z} = \sum_{n,m=1}^{\infty} C_{nm} \cdot \cos\left({}^{\pi n x}/_{d_x}\right) \cdot \cos\left({}^{\pi m y}/_{d_y}\right) \cdot \gamma e^{\gamma z}\left(1 + e^{2\gamma(l-z)}\right) \Bigg|_{z=0} = \begin{cases} 0, for & (A.10, a-d) \\ -\frac{q}{\lambda}, for & (A.9) \end{cases} \tag{A.17}$$

Next step is determination of coefficients $C_{n,m}$.

In hot zone, we have:

$$\sum_{n,m=1}^{\infty} C_{nm} \cdot \cos\left(\pi nx/_{d_x}\right) \cdot \cos\left(\pi my/_{d_y}\right) \cdot \gamma\left(1+e^{2\gamma l}\right) = -\frac{q}{\lambda} \tag{A.18}$$

Multiplying (A.18) with $\cos\left(\pi nx/_{d_x}\right) \cdot \cos\left(\pi my/_{d_y}\right) \int_{-L}^{L}\int_{-W}^{W} dxdy$ and integrating from $-d_x$ to d_x and $-d_y$ to d_y we get:

$$\sum_{n,m=1}^{\infty} C_{nm} \int_{-d_x}^{d_x} \cos^2\left(\pi nx/_{d_x}\right)dx \int_{-d_y}^{d_y} \cos^2\left(\pi my/_{d_y}\right)dy \cdot \gamma\left(1+e^{2\gamma l}\right) = -\frac{q}{\lambda} \int_{-L}^{L} \cos\left(\pi nx/_{d_x}\right)dx \int_{-W}^{W} \cos\left(\pi my/_{d_y}\right)dy \tag{A.19}$$

Let us solve every integral in (A.19) separately.

$$\int_{-d_x}^{d_x} \cos^2(x)dx = \int_{-d_x}^{d_x} \frac{1+\cos(2x)}{2}dx = d_x + \frac{1}{2}\left(\sin(2d_x) - \sin(-2d_x)\right) = d_x + \sin(2d_x) = d_x + \sin\left(\frac{2\pi nd_x}{d_x}\right) = dx$$

Analogously, $\int_{-d_y}^{d_y} \cos^2(y)dy = dy$.

On the right side of equation (A.19): $\int_{-L}^{L} \cos\left(\pi nx/_{d_x}\right)dx = \frac{d_x}{n\pi}\sin\left(\pi nx/_{d_x}\right)\Big|_{-L}^{L} = \frac{2d_x}{n\pi}\sin\left(\pi nL/_{d_x}\right)$ and

$$\int_{-W}^{W} \cos\left(\pi my/_{d_y}\right)dy = \frac{2d_y}{m\pi}\sin\left(\pi mW/_{d_y}\right)$$

After all, equation (A.19) will have a form:

$$C_{nm} \cdot d_x d_y \cdot \gamma\left(1+e^{2\gamma l}\right) = -\frac{q}{\lambda} \cdot \frac{2d_x}{n\pi} \cdot \frac{2d_y}{m\pi} \sin\left(\pi nL/_{d_x}\right)\sin\left(\pi mW/_{d_y}\right),$$

Finally, after cancellation of d_x and d_y, the coefficients C_{nm} can be found with formula:

$$C_{nm} = -\frac{q}{\lambda} \cdot \frac{4/_{\pi^2 nm}}{\gamma\left(1+e^{2\gamma l}\right)} \sin\left(\pi nL/_{d_x}\right)\sin\left(\pi mW/_{d_y}\right) \tag{A.20}$$

No we need to consider the case of zero eigenvalues of α, β and γ.

There three possible combinations:

1) $\alpha = 0$, $\beta_m = m\pi/_{d_y}$ $(\beta \neq 0)$. $\gamma^2 = \beta^2 = \pi^2\left(\frac{m}{d_y}\right)^2$ (A.21)

2) $\alpha_n = n\pi/_{d_x}$, $\beta = 0$. $\gamma^2 = \alpha^2 = \pi^2\left(\frac{n}{d_x}\right)^2$ (A.22)

3) $\alpha = 0$, $\beta = 0$, $\gamma = 0$ (A.23)

Note, that the case $\alpha \neq 0$, $\beta \neq 0$, $\gamma = 0$ not possible due to the relation $\gamma^2 = \alpha^2 + \beta^2$.

For the case, described by equations (A.21), first of equations (A.4) will be modified as: $X'' = 0$; $X' = k = 0$; $X = kx + b = b$, which is included into the general constant.

Then, solution for this case can be written as

$$T_2 \sim \cos(\beta y)\cdot\left(ce^{\gamma z} + de^{-\gamma z}\right) \Rightarrow \sum_{m=1}^{\infty} C_m \cos\left({}^{\pi m y}/_{d_y}\right)\cdot e^{\gamma z}\left(1 - e^{2\gamma(l-z)}\right). \tag{A.24}$$

$$\frac{\partial T_2}{\partial z} = \sum_{m=1}^{\infty} C_m \cos\left({}^{\pi m y}/_{d_y}\right)\cdot \gamma e^{\gamma z}\left(1 + e^{2\gamma(l-z)}\right)\Bigg|_{z=0} = \begin{cases} 0, for & (A.10, a-d) \\ -\dfrac{q}{\lambda}, for & (A.9) \end{cases}$$

Multiplying by $\int_{-d_y}^{d_y} \cos\left({}^{\pi m y}/_{d_y}\right)dy \int_{-d_x}^{d_x} dx$ and integrating as in general case, we obtain the value of constant:

$$C_m = -\frac{qL}{\lambda d_x}\cdot\frac{{}^{2}/_{\pi m}}{\gamma\left(1 + e^{2\gamma l}\right)}\sin\left({}^{\pi m W}/_{d_y}\right) \tag{A.25}$$

Performing the same procedure for conditions (A.22) and (A.23) we can build all separable solutions:

$$T_1(x,y,z) = \sum_{n,m=1}^{\infty}\left(-\frac{q}{\lambda}\right)\frac{{}^{4}/_{\pi^2 nm}}{\gamma\left(1+e^{2\gamma l}\right)}\cdot e^{\gamma z}\left(1 - e^{2\gamma(l-z)}\right)\sin\left({}^{\pi n L}/_{d_x}\right)\sin\left({}^{\pi m W}/_{d_y}\right)\cdot\cos\left({}^{\pi n x}/_{d_x}\right)\cos\left({}^{\pi m y}/_{d_y}\right) \tag{A.26}$$

$$T_2(y,z) = \sum_{m=1}^{\infty}\left(-\frac{q}{\lambda}\right)\frac{2Ld_y}{\pi^2 m^2 d_x}\frac{1 - e^{{}^{2\pi m(l-z)}/_{d_y}}}{1 + e^{{}^{2\pi m l}/_{d_y}}}\cdot e^{{}^{\pi m z}/_{d_y}}\sin\left({}^{\pi m W}/_{d_y}\right)\cos\left({}^{\pi m y}/_{d_y}\right) \tag{A.27}$$

$$T_3(x,z) = \sum_{n=1}^{\infty}\left(-\frac{q}{\lambda}\right)\frac{2Wd_x}{\pi^2 n^2 d_y}\frac{1 - e^{{}^{2\pi n(l-z)}/_{d_x}}}{1 + e^{{}^{2\pi n l}/_{d_x}}}\cdot e^{{}^{\pi n z}/_{d_x}}\sin\left({}^{\pi n L}/_{d_x}\right)\cos\left({}^{\pi n x}/_{d_x}\right) \tag{A.28}$$

$$T_4(z) = \left(-\frac{q}{\lambda}\right)\frac{WL}{d_x d_y}(z - l) \tag{A.29}$$

The general solution is obtained by summation of (A.26)-(A.29):

$$T(x,y,z) = T_1(x,y,z) + T_2(y,z) + T_3(x,z) + T_4(z) \tag{A.30}$$

Acknowledgements

I would like to acknowledge the contribution of my partners to the results presented in the frame of this work:

Dr. S. Vitusevich, Dipl.-Phys. A. Kurakin
ISG-2, Forschungszentrum Jülich, Germany

Prof. A.E. Belyaev, Dr. V. Sokolov, Prof. V.A. Kochelap, Prof. R. Konakova
Institute of Semiconductor Physics, National Academy of Science of Ukraine, Kiev, Ukraine

Prof. A.E. Danilchenko
Institute of Physics, National Academy of Science of Ukraine, Kiev, Ukraine

Dr. M.V. Petrychuk
Taras Shevchenko National University, Kiev, Ukraine

Dr. V.Kaper, Dr.V.Tilak, Prof. L.F.Eastman , Dr J.R.Shealy
School of Electrical Engineering, Cornell University, Ithaca, New York, U.S.A

This work has been partially funded by the Office of Naval Research under contract No. N00014-01-1-0828 (monitored by Dr. Colin E.C. Wood).

Publications

Results that were gained in the frame of this work have been published or will be published in the following articles:

1 Excess low-frequency noise in AlGaN/GaN-based high-electron-mobility transistors. S.A. Vitusevich, S.V.Danylyuk, N.Klein, M.V.Petrychuk, V.N.Sokolov, V.A.Kochelap, A.E.Belyaev, V.Tilak, J.Smart, A.Vertiatchikh and L.F.Eastman. Appl. Phys. Lett., V.80(n.12), (2002), p.2126-2128.

2 Low-frequency noise in AlGaN/GaN high electron mobility transistors irradiated by γ-Ray Quanta. S.A.Vitusevich, N.Klein, M.V.Petrychuk, A.E.Belyaev, S.V.Danylyuk, R.V.Konakova, A.Yu.Avksentiev, B.A.Danilchenko, V. Tilak, J. Smart, A. Vertiatchikh and L. F. Eastman. Proc. International Workshop on Nitride Semiconductors (IWN 2002), 22-25 July, Aachen, Germany, (2002), p.269

3 Two-dimensional electron dynamics in GaN/AlGaN heterostructures. S.A. Vitusevich, S.V. Danylyuk, and N. Klein , M.V. Petrychuk, A.Yu.Avksentiev, V.N. Sokolov, V.A. Kochelap, and A.E. Belyaev , V. Tilak, J. Smart, A. Vertiatchikh and L. F. Eastman. Proc. International Workshop on Nitride Semiconductors (IWN 2002), 22-25 July, Aachen, Germany, (2002), p.309

4 The study of excess low-frequency noise sources in nitride-based high-electron-mobility transistors. S.A. Vitusevich, S.V. Danylyuk, N. Klein , M.V. Petrychuk, V.N. Sokolov, V.A. Kochelap, A.E. Belyaev, V. Tilak, J. Smart, A. Vertiatchikh and L. F. Eastman. Proc. 26th International Conference on the Physics of Semiconductors (ICPS26), July 29-August 2, Edinburgh, UK, (2002), Part.III, p.233

5 Low-frequency noise in AlGaN/GaN high electron mobility transistors irradiated by γ-Ray Quanta. S.A.Vitusevich, N.Klein, M.V.Petrychuk, A.E.Belyaev, S.V.Danylyuk, R.V.Konakova, A.Yu.Avksentiev, B.A.Danilchenko, V. Tilak, J. Smart, A. Vertiatchikh and L. F. Eastman. Phys. Stat. Sol.(c), V.0 (N.1),(2002) p.78-81.

6 Two-dimensional electron dynamics in GaN/AlGaN heterostructures. S.A. Vitusevich, S.V. Danylyuk, and N. Klein , M.V. Petrychuk, A.Yu.Avksentiev, V.N. Sokolov, V.A. Kochelap, and A.E. Belyaev , V. Tilak, J. Smart, A. Vertiatchikh and L. F. Eastman. Phys. Stat. Sol.(c), V.0 (N.1),(2002) p.401-404.

7 The study of excess low-frequency noise sources in nitride-based high-electron-mobility transistors. S.A. Vitusevich, S.V. Danylyuk, N. Klein, M.V. Petrychuk, V.N. Sokolov, V.A. Kochelap, A.E. Belyaev, V. Tilak, J. Smart, A. Vertiatchikh and L. F. Eastman. Proc. 26th International Conference on the Physics of Semiconductors (ICPS26), July 29-August 2, Edinburgh, UK, (2002),(5 pages, P171, the ICPS26 proceedings on CD).

8 Separation of Hot-Electron and Self-Heating Effects in Two-Diensional AlGaN/GaN-Based Conductivity Channels" by S.A. Vitusevich, S.V.Danylyuk, N. Klein, M.V.Petrychuk, A.Yu.Avksentiev,V.N.Sokolov, V.A.Kochelap, A.E. Belyaev, V.Tilak, J.Smart, A.Vertiatchikh, L.F.Eastman, Appl. Phys. Lett., V.82(N.5), (2003), p.748-750.

9 The investigation of properties of electron transport in AlGaN/GaN heterostructures. S.V.Danylyuk, S.A.Vitusevich, B.Podor, A.E.Belyaev, V.Tilak, J.Smart, A.Vertiatchikh, L.F.Eastman. Proc. 4th International Conference on Low Dimensional Structures and Devices, December 8-13, Fortaleza-Ceara, Brazil(2002), p. PS-I-17.

10 The investigation of properties of electron transport in AlGaN/GaN heterostructures. S.V.Danylyuk, S.A.Vitusevich, B.Podor, A.E.Belyaev, A.Yu.Avksentyev, V.Tilak, J.Smart, A.Vertiatchikh, L.F.Eastman. Microelectronics Journal, V.34 (2003), p.575-577.

11 Barrier material improvement in AlGaN/GaN microwave transistors under gamma irradiation treatment. S.A.Vitusevich, M.V.Petrychuk, N. Klein, S.V.Danylyuk, A.E.Belyaev, R.V.Konakova, A.Yu.Avksentiev, B.A.Danilchenko, V.Tilak, J.Smart, A. Vertiatchikh and L.F. Eastman. Proc. of Mat.Res. Soc. Symp.(MRS Spring Meeting),San Francisco, April 21-25, (2003), p.183.

12 Hot-electron transport in III-V nitride based two-dimensional gases. S. A. Vitusevich, S. V. Danylyuk, B. A. Danilchenko, N. Klein, S. E. Zelenskyi, A. P. Budnik, R.V. Didenko, A. Yu. Avksentyev, V. N. Sokolov, H. Lüth, V. A. Kochelap, and A.E. Belyaev. Proc. 5th International Conference on Nitride Semiconductors (ICNS-5), May 25-30, 2003, Nara, Japan (2003), p.174.

13 Peculiarities of low frequency noise in GaN-based high electron mobility transistors. S.A.Vitusevich, M.V.Petrychuk, N.Klein, S.V.Danylyuk, P.Javorka, M.Marso, P.Kordos, H.Lüth. Proceedings of the 17th International Conference "Noise and Fluctuations ICNF 2003", August 18-22, Prague, 2003. Editor. Josef Sikula. ISBN 80-239-1005-1, pp.789-792.

14 Hot-electron transport in III-V nitride based two-dimensional gases. S. A. Vitusevich, S.V. Danylyuk, B. A. Danilchenko, N. Klein, S. E. Zelenskyi, A. P. Budnik, R. V.

Didenko, A. Yu. Avksentyev, V. N. Sokolov, H. Lüth, V. A. Kochelap, and A.E. Belyaev. Phys. Stat. Sol. (C). V.0. N.7. (2003), p.2408-2411.

15 Equilibrium and non- equilibrium *1/f* noise in AlGaN/GaN TLM structures. Vitusevich S.A., Danylyuk S.V., Petrychuk M.V., Antoniuk O.A., Klein N., Belyaev.A.E. Proc. 1st International Meeting on Applied Physics (APHYS-2003), Badajoz, Spain, October 13-18, (2003), p.620

16 Ultra-high electric field transport in GaN-based heterostructures. S.A.Vitusevich, S.V.Danylyuk, B.A.Danilchenko, N.Klein, S.E.Zelenskyi, A.P.Budnik, A.Yu.Avksentyev, N.V.Sokolov, V.A.Kochelap, A.E.Belyaev, M.V.Petrychuk, H.Lüth. Proc. International Semiconductor Device Research Symposium (ISDRS03), December 10-12, 2003,Washington, DC, p.108-109

17 Equilibrium and non-equilibrium *1/f* noise in AlGaN/GaN TLM structures. S.A.Vitusevich, S.V.Danylyuk, M.V.Petrychuk, O.A.Antoniuk, N.Klein, A.E.Belyaev. Journal of Applied Physics (accepted for publication).

18 Phase Noise Study of an AlGaN/GaN HEMT X-Band Oscillator. S.V.Danylyuk, S.A.Vitusevich, V.Kaper, V.Tilak, N.Klein, J.R.Shealy. Proc. International Workshop on Nitride Semiconductors (IWN 2002), 19-24 July, Pitsburgh, USA, (2004), p.24

Special thanks

On this page I want to thank all people who directly or indirectly made this work possible. Their help, support and advices were the driving force to my advancements on scientific path.

First of all, I want to thank Prof. Dr. Hans Lüth for the opportunity to realize this work at the Institute of Thin Films and Interfaces (ISG) of the Research Centre Jülich, Germany.

My special thanks go to Dr. Svetlana Vitusevich for providing me with excellent guidelines for my work. Countless hours of discussions, constant attention to my results, generous help in all scientific or not situations – without all of these present work would never be done.

Also I want to thank Priv. Doz. Dr. Norbert Klein for numerous interesting discussions and his kind agreement to review this work.

With gratitude I want to acknowledge all colleagues at the ISG-1 and ISG-2 institutes, Dr. B.B.Jin, A. Kurakin, A. Rebikov, O.Antoniuk, Dr. P. Lahl, Dr. A. Klushin, Dr. R. Wördenweber, Dr. R. Ott, Dr. E. Hollmann, Dr. P. Jaworka, Dr. M. Mikulics, Dipl.-Ing. J. Bernát, Dr. M.J. Wolter, Dr. M. Kocan, Dr. M. Indlekofer, Dr. S. Montanari, Dr. R. Adam, Dr. M. Lepsa, Dr. M. Marso and Prof. P. Kordos for their friendly collaboration and help.

Especially I want to thank Dipl.-Phys. Michael Schuster and Dipl.-Phys. Diego Cassel for friendly support at work and in private life and for everyday fruitful and interesting discussions.

I also want to thank tremendous cleanroom staff, namely: S. Bunte, Dipl.-Ing. F. Ringelmann, Dipl.-Ing. A. Steffen, H.-W. Wingens, J. Müller, J. Zillikens, M. Nonn und A. Pracht.

Heartfelt gratitude goes to Clarissa Jansen, Irene Schumacher, Mirjam Gruber and H.-B. Ix for perfect managing of administrative things.

My cordial thanks goes to my extraordinary parents, whose support and understanding during all my life created wonderful possibilities for my personal and scientific growth.

Finally I would like to thank my beautiful wife Nataliya for creating nice family atmosphere that helps me greatly during this work. Without her my life and this work would not have been complete.

References

[1] Manfra, M.J.; Weimann, N.G.; Hsu, J.W.P.; Pfeiffer, L.N.; West, K.W.; Syed, S.; Stormer, H.L.; Pan, W.; Lang, D.V.; Chu, S.N.G.; Kowach, G.; Sergent, A.M.; Caissie, J.; Molvar, K.M.; Mahoney, L.J.; Molnar, R.J., J. Appl. Phys., **92**, 338 (2002)

[2] Sullivan, G.J.; Higgins, J.A.; Chen, M.Y.; Yang, J.W.; Chen, Q.; Pierson, R.L.; McDermott, B.T., Electronics Letters, **34**, 9, 1998. p.922-4.

[3] L. Shen, R. Coffie, D. Buttari, S. Heikman, A. Chakraborty, A. Chini, S. Keller, S.P. DenBaars, and U. K. Mishra., IEEE Electron Dev. Lett., **25**, 1, 2004. p.7-9.

[4] Sheppard, S.T.; Doverspike, K.; Pribble, W.L.; Allen, S.T.; Palmour, J.W.; Kehias, L.T.; Jenkins, T.J., IEEE Electron Device Letters, **20**, 4, 1999. p.161-3.

[5] A. Van der Ziel, *Noise*, New Jersey:Prentice Hall (1954)

[6] A. Van der Ziel, *Noise, Sources, Characterisation, Measurements*, New Jersey:Prentice Hall (1970)

[7] M.J. Buckingham, Noise in Electronic Devices and Systems, New-York – Brisbane – Chichester – Ontario: Ellis Horwood Ltd. (1983)

[8] N. Wiener, Acta Math., **55**, 117 (1930)

[9] A. Khintchine, Math. Ann., **109**, 604 (1934)

[10] A. Einstein, Ann. d. Phys., **19**, 371 (1906)

[11] G.H. de Haas-Lorentz, *Die Brownsche Bewegung und einige verwandte Erscheinungen*, Braunschweig (1913)

[12] W. Schottky, Ann. d. Phys. **57**, 541 (1918)

[13] Van der Ziel, *Noise in solid state devices and circuits*, New-York – Chichester – Brisbane –Toronto-Singapore: John Wiley & Sons, Inc. (1986)

[14] AIP Conf. Proc., **285**, *"Noise in Physical Systems and 1/f Fluctuations"*, St.Louis, August 1993, P.H. Handel and A.L. Chung, Eds. New York: AIP Press (1993)

[15] Proc. 11^{th} Int. Conf. On Noise in Physical Systems and 1/f Fluctuations, Kyoto, Nov. 1991, T.Musha, S.Sato, and M.Yamamoto, Eds. Tokyo:Ohmsha Ltd. (1991).

[16] J.A. Garrido, B.E. Foutz, J.A. Smart, J.R. Murphy, W.J. Schaff, L.F. Eastman, Appl. Phys. Lett., **76,** 3442 (2000).

[17] A.L. MacWhorter, in *Semiconductor Surface Physics,* Ed. R.H. Kingston, Philadelphia, PA, Univ. of Philadelphia Press, 207 (1957).

[18] F.N.Hooge, T.G.M. Kleinpenning, and L.K.J.Vandamme, Rep.Prog.Phys.**44**, 479 (1981)

[19] A.L. McWhorter, PhD Thesis, Massaxhussetts Institute of Technology, Cambridge, Mass. (1955)

[20] A.L. McWhorter, Semicond. Surf. Physics, ed. R.H. Kingston, Philadelphia: University of Pennsylvar Press, 207 (1957)

[21] R.F. Voss, J. Clarke, Phys. Rev. B **13**, 556 (1976)

[22] F.N. Hooge, Phys. Lett., **29A**, 139 (1969)

[23] A.M.H. Hoppenbrouwers, F.N. Hooge, Philips Res. Rep., **25**, 69 (1970)

[24] F.N. Hooge, A.M.H. Hoppenbrouwers, Physica, **45**, 386 (1969)

[25] P. Dutta, P.M. Horn, Rev. Modern Phys., **53**, 497,1981

[26] P.J. Handel, Phys. Rev. Lett., **34**, 1492 (1975)

[27] G.S.Kousik, C.M. van Vliet, G. Bosman, P.Handel, Advances in Physics, **34**, 663 (1985)

[28] P H.Handel, T.H. Chung, in [14],p 176

[29] P.H. Hooge, IEEE Trans. On Elect. Devices, **41**, N11, 1926 (1994)

[30] O. Ambacher, B. Foutz, J. Smart, J.R. Shealy, N.J. Weimann, K. Chu, M. Murphy, A.J. Sierakowski, W.J. Schaff, and L. F. Eastman, J. Appl. Phys. **87,** 334 (2000).

[31] S.J.Pearton, J.C. Zolper, R.J. Shul, F. Ren, J. Appl. Phys. **86**, 1 (1999).

[32] B.K.Ridley, J. Appl. Phys. **90**, 6135 (2001).

[33] R. Gaska, A. Osinsky, J. W. Yang, and M.S. Shur, IEEE Electron Device Lett. **19**, 89 (1998).

[34] M. Kuball, J.M. Hayes , M.J. Uren, T. Martin, J.C.H. Birbeck, R.S. Balmer, and B.T. Hughes, IEEE Electron Device Lett. **23**, 7 (2002).

[35] T.-H. Yu and K.F. Brennan, J. Appl. Phys. **91**, 3730 (2002).

[36] R. Dennemeyer, *Introduction to Partial Differential Equations and Boundary Value Problems*, New York: McGrow-Hill Book Company, Ch.3, pp.149-150 (1968)

[37] J.R.Shealy, V.Kaper, V.Tilak, T. Prunty, J.A.Smart, B.Green and L.F.Eastman, J. Phys. : Condens. Matter **14**, 3499 (2002).

[38] S. A. Vitusevich et al, Appl. Phys. Lett., **82**, 748 (2003).

[39] J.J.Harris, K.J.Lee, T.Wang, S.Sakai, Z.Bougrioua, I.Moerman, E.T.Thrush, J.B.Webb, H.Tang, T.Martin, D.K.Maude, J-C.Portal, Semicond. Sci. and Technol., **16**, 402 (2001).

[40] P.T.Coleridge, Phys.Rev. B, **44,** 8, 3793 (1991).

[41] A. Koudymov, H. Fatima, G. Simin, J. Yang, M. Asif Khan, A. Tarakji, X. Hu, M.S. Shur, and R. Gaska, Appl. Phys. Lett., **80**, 3216 (2002).

[42] W Ted Masselink, Semicond. Sci. Technol. **4**, 512 (1989).

[43] N.M. Stanton, P. Hawker, A.J. Kent, T.S. Cheng, and C.T. Foxon, Phys. stat. sol. (a) **176**, 369 (1999).

[44] S. J. Pearton, F. Ren, A. P. Zhang, and K. P. Lee, Material Sci. Eng. R **30,** 55 (2000).

[45] E.G.Brazel, M.A.Chin, and V.Narayanamurti, Appl. Phys. Lett., **74**, 2367 (1999).

[46] J.W.P.Hsu, M.J.Manfra, D.V.Lang, S.Richter, S.N.G.Chu, A.M.Sergent, R.N.Kleiman, L.N.Pfeiffer, and R.J.Molnar, Appl. Phys. Lett., **78**, 1685 (2001).

[47] J.W.P.Hsu, M.J.Manfra, R.J.Molnar, B.Heying, J.S.Speck, Appl. Phys. Lett., **81**, 79 (2002).

[48] S. Rumyantsev, M.E. Levinshtein, R. Gaska, M.S. Shur, J.W. Yang, and M.A. Khan, J. Appl. Phys.; **87**; 1849 (2002)

[49] M.E. Levinshtein, S.L. Rumyantsev, M.S. Shur, R. Gaska, M. Asif Khan, IEE Proc.-Circuits, Devices and Systems, **149**, 32-39 (2002) .

[50] J. A. Garrido, B. E. Foutz, J. A. Smart, J. R. Shealy, M. J. Murphy, W. J. Schaff, L.F. Eastman, E. Munoz, Appl. Phys. Lett., **76**, 3442 (2000).

[51] J. A. Garrido, F. Calle, E. Mu˜noz, I. Izpura, J. L. Sanchez-Rojas, R. Li and K. L. Wang Electron. Lett., **34**, 2357 (1998).

[52] A. Balandin, S. V. Morozov, S. Cai, R. Li, K. L. Wang, G. Wijeratne and C.R. Viswanathan, IEEE Trans. Microwave Theory Tech., **47**, 1413 (1999).

[53] N. Pala, R. Gaska, S. Rumyantsev, M. S. Shur, M. A. Khan, X. Hu, G. Simin and J. Yang, Electron. Lett., **36**, 268 (2000).

[54] V.A. Kochelap, V.N. Sokolov, O.M. Bulashenko, J.M. Rubí, Appl. Phys. Lett., **78**, 2003 (2001)

[55] F.N. Hooge, Physica B, **311**, 238 (2002)

[56] B.K. Ridley, J. Appl. Phys., **90**, 6135 (2001)

[57] A. Van der Ziel, *Noise in solid state devices and circuits,* John Wiley & Sons, New York (1986).

[58] F.A. Ponce, D.P. Bour, W. Gotz, P.J. Wright, Appl. Phys. Lett. **68**, 57, (1996).

[59] J.W.P. Hsu, M.J. Manfra, R.J. Molnar, B. Heying, J.S. Speck, Appl. Phys. Lett., **81,** 79 (2002).

[60] J.W.P. Hsu, M.J. Manfra, D.V. Lang, S. Richter, S.N.G. Chu, A.M. Sergent, R.N. Kleiman, L.N.Pfeiffer, R.J. Molnar, Appl. Phys. Lett., **78**, 1685 (2001).

[61] B. Luo, J.W. Johnson, F. Ren, K.K. Allums, C.R. Abernathy, S.J. Pearton, A.M. Dabiran, A.M. Wowchak, C.J. Polley, P.P. Chow, D. Schoenfeld, A.G. Baca, Appl. Phys. Lett., **80,** 604 (2002).

[62] S.L. Rumyantsev, N. Pala, M.S. Shur, E. Borovitskaya, A.P. Dmitriev, M.E. Levinshtein, R. Gaska, M.A. Khan, J. Yang, X. Hu and G. Simin, IEEE Trans. Electron. Devices. **48**, 530 (2001).

[63] A.E. Belyaev, J. Breza, E.F. Venger, M. Vesely, I. Yu. Il'in, R.V. Konakova, J. Liday, V.G. Lyapin, V.V. Milenin, I.V. Prokopenko, Yu.A. Tkhorik, *Radiation resistance of GaAs-based microwave Schottky-barrier devices,* Kiev: Interpress Ltd. (1998)

[64] G.H.Olsen, M.Ettenberg, J. Appl. Phys., **48**, 2543 (1977).

[65] A.V.Vertiatchikh, L.F.Eastman, W.J.Schaff, T.Prunty, Elect. Lett., **38**, 388 (2002).

[66] R.Tompson, T.Prunty,V.Kaper,J.R.Shealy. IEEE Trans. on Elect. Device, **51**, 292 (2004).

[67] H.J.Siweris, B.Schiek, IEEE Trans. On Microwave Theory and Techniques, **33,** 233 (1985).

[68] D.B. Leeson, in Proc.IEEE, **54**, 329 (1966).

[69] D.B. Leeson. *Proc. IEEE.* **54**, 329 (1966).

[70] H.Rhodin, C.Su and C.Stolte, Proc. 1984 IEEE MTT-S, 267 (1984).

[71] M.N.Tutt, D.Pavlidis, A.Khatibzadeh, B.Bayraktarogly. IEEE Trans. On Microwave Theory and Techniques, **43**, 1461 (1995).

[72] J.B.Shealy, J.A.Smart and J.R.Shealy. IEEE Microwave and Wireless Component Letters. **11**, 244 (2001).

CURRICULUM VITAE

Serhiy Danylyuk

Date	Events
25.07.1978	Was born in Prilutske village of Volyn region of Ukraine
01.09.1984	Started study in Prilutske school
01.09.1990	Move to Lutsk city and continue study in Lutsk general school #7
27.06.1994	Finished general school #7
01.09.1994	Enter the Volyn State University at Physics faculty
23.06.1999	Completed M.S. in physics at Volyn State University
17.11.2000	Started work as a scientist in Institute of Semiconductor Physics NAS Ukraine, Kiev
03.10.2001	Started as PhD-student in Forschungszentrum Jülich, Germany

Forschungszentrum Jülich
in der Helmholtz-Gemeinschaft

Jül-4165
Februar 2005
ISSN 0944-2952